

Methods for Nitrogen Activation by Reduction and Oxidation

H. Iriawan[†], S.Z. Andersen[†], X. Zhang, B. M. Comer, J. Barrio, P. Chen*, A.J. Medford*, I.E.L. Stephens*, I. Chorkendorff*, Y. Shao-Horn*

[†] These authors have contributed equally

*Corresponding authors

Abstract

200 words maximum

The industrial Haber-Bosch process for the production of ammonia (NH_3) is crucial for modern society. The process has significant drawbacks, as it is highly energy intensive due to the inherent challenge of activating N_2 , not sustainable due to substantial CO_2 emissions, and requires large-centralized facilities. New strategies of sustainable N_2 fixation, such as low-temperature thermochemical catalysis and (photo)electrocatalysis, have been pursued over the past few decades, but progress has been hindered by the lack of rigor and reproducibility in the collection and analysis of results. In this Primer, we provide a holistic step-by-step protocol, applicable to all nitrogen-transformation reactions, focused on verifying genuine N_2 activation by accounting for all contamination sources. We compare state-of-the-art results from different catalytic reactions following the protocol's framework, and discuss necessary reporting metrics and ways to interpret both experimental and density functional theory results. This Primer covers various common pitfalls in the field, best practices to improve reproducibility and rigor, and cost-efficient ways to carry out rigorous experimentation. The future of nitrogen catalysis will require an increase in rigorous experimentation and standardization to prevent false positives from appearing in the literature, and help the field advance towards practical technologies for the activation of N_2 .

[H1] Introduction

[H2] Importance of Ammonia for World Population Growth

Nitrogen is essential to all forms of life, and constitutes ~78 % of air in the form of dinitrogen (N₂). However, the formidable strength of the N≡N triple bond (9.79 eV)¹ makes N₂ fixation into biologically-available forms extremely difficult². N₂ fixation in nature occurs in two ways. Lightning can convert N₂ in air to nitrous oxides (NO_x)³. More dominantly, nitrogenase enzymes can catalyze N₂ reduction to ammonia (NH₃) by a multi-electron transfer process. The latter process involves the hydrolysis of at least 16 equivalents of adenosine triphosphate (ATP) to produce 2 molecules of NH₃ and at least 1 molecule of dihydrogen (H₂), performing at up to 65% selectivity at 1 atm N₂ in the absence of N₂O inhibitors^{4,5}. Yet, biological N₂ fixation is kinetically slow due to reliance on electron tunnelling⁶ and is insufficient to sustain intensive modern agricultural practices⁷.

Prior to industrial production of NH₃ by the Haber-Bosch process, natural fertilizers came in the form of caliche from Chile and guano from Peru⁸. In 1898, Sir William Crookes warned mass starvation as the biggest challenge of the 20th century⁹, instigating the burgeoning interest in industrial N₂ activation. In 1903, the Birkeland-Eyde process became commercial⁷, utilizing electric arcs to fix atmospheric N₂ into nitric acid (HNO₃), based on a method used by Henry Cavendish in 1784¹⁰. In 1908, Fritz Haber managed to synthesize NH₃ from N₂ and H₂ (N_{2(g)} + 3H_{2(g)} ⇌ 2NH_{3(g)}, ΔG° = -32.9 kJ/mol¹¹, eq. 1) on a table-top machine, but it suffered from remarkably slow kinetics under standard temperature and pressure⁸. To boost the formation rate of NH₃ and tilt the equilibrium, Haber increased both temperature and pressure over an Os catalyst⁷. Subsequently, BASF bought the invention and Carl Bosch up-scaled the production in 1913⁷ to the currently known Haber-Bosch process, which operates at 400-450 °C and 150-250 bar over a multi-promoted fused Fe catalyst¹². A more active Ru-based supported catalyst was later developed, but was not as widely adopted due to cost and stability drawbacks¹³. Gerhard Ertl elucidated the molecular details of the catalytic N₂ reduction to NH₃ over Fe, enriching mechanistic understanding of the system¹⁴, and received a Nobel Prize in 2007 (Figure 1).

Today industrial NH₃ production by the Haber-Bosch process is the backbone of modern society and is responsible for the population boom in the 20th century¹⁵⁻¹⁷. Current annual NH₃ production exceeds 180 million metric tonnes¹⁸ (Mt) globally, and its primary use is artificial fertilizers (~80 %¹⁹), sustaining two fifths of the global population²⁰. Additionally, NH₃ is the source of every N atom in all synthetic chemicals²¹, a key reactant in the chemical industry²², and a potential hydrogen energy carrier^{23,24}. However, NH₃ production from the Haber-Bosch process is energy and emission intensive. Nearly all the required energy and emissions in NH₃ production originate from the generation of H₂, most commonly from natural gas via steam-methane reforming²⁵ (0.75CH_{4(g)} + 1.5H_{2O(l)} ⇌ 3H_{2(g)} + 0.75CO_{2(g)}, ΔG° = +98.0 kJ/mol¹¹, eq. 2). For the methane-fed process, NH₃ production has a theoretical minimum energy input of 22.2 GJ/t_{NH₃} along with the stoichiometric emission 1.2 t_{CO₂}/t_{NH₃}¹². In comparison, modern NH₃ production plants using the best available technology consume 28-33 GJ/t_{NH₃} and emit 1.6 t_{CO₂}/t_{NH₃}^{12,25} (although the global average is 2.9 t_{CO₂}/t_{NH₃}²⁶ due to the use of coal and oil-based feedstocks¹²). At >180 Mt annually, global NH₃ production therefore consumes about 1% of total world energy and emits 1.4% of global CO₂ emissions^{25,27}. Implementation of CO₂ sequestration processes or other carbon offsets can reduce emissions but will add cost, plant complexity, and energy losses²⁸. Reducing reliance on fossil fuels to address climate change challenges calls for sustainable alternatives for NH₃ production.

[H2] Concepts and challenges to decarbonize N₂ activation

Replacing the generation of H₂ by steam-methane reforming with renewable water splitting (3H₂O_(l) \rightleftharpoons 3H_{2(g)} + 1.5 O_{2(g)}, $\Delta G^\circ = +711.4$ kJ/mol¹¹, eq. 3) can eliminate CO₂ emissions associated with the Haber-Bosch process²⁹, referred to as Gen 2 (Figure 1), resulting in an energy expenditure of $\Delta G^\circ = +678.5$ kJ/mol¹¹ for N_{2(g)} + 3H_{2O(l)} \rightleftharpoons 2NH_{3(g)} + 1.5 O_{2(g)} (eq. 4). Operating the Haber-Bosch at reduced temperatures and pressures and coupling with renewable H₂ production via water electrolysis could make NH₃ production sustainable and reduce capital cost via smaller, local reactors. However, several major challenges need to be addressed³⁰, including: synthesizing NH₃ at milder conditions (pressures of 20-40 bar) to cope with the intermittent and low-pressure influent of H₂ from water electrolysis; sustainable separation of pure N₂ from air, as N₂ is presently separated from O₂ by combustion of unreacted methane; and the discovery of low-temperature thermochemical catalysts to achieve high yield per pass at moderate pressures.

Electrochemical reduction of N₂ and H₂O to make NH₃ is appealing, as NH₃ can be synthesized directly at the point of consumption, eliminating transportation cost and emissions and reducing issues of excess fertilizer run-off^{31,32}. The energy expenditure of $\Delta G^\circ = +678.5$ kJ/mol_{N2 fixed} (eq. 4) or 19.9 GJ/t_{NH3} for such process can be provided by using (photo)electrochemical systems powered by solar or wind (Gen 3, see Figure 1). This process can be made sustainable and economical,^{33,34} where 40 m² of state-of-the-art solar cells operating at 20% efficiency are required to meet the average nutrient requirement of 100 kg of fixed nitrogen (expressed as monatomic N) per hectare of land per year, by assuming 5% electrical-to-NH₃ efficiency (the calculation neglects upstream and downstream separations, see Supplementary Information for details). The current densities will need to be comparable to those of the state-of-the-art electrolyzers to keep down capital costs; the US Department of Energy have a target³⁵ of 300 mA cm⁻²_{geo} at 90% Faradaic efficiency.

The reduction of N₂ can also be facilitated by non-thermal plasmas, where vibrational excitations of ground-state N₂ via collision with high-energy electrons can decrease the N₂ activation barriers³⁶. Typically, microwave and dielectric barrier discharge (DBD) reactors have been used, where the NH₃ synthesis rate can be increased through heterogeneous catalysis³⁷. Kim *et al.* have reported among the highest energy efficiencies of 25-35 g_{NH3} kWh⁻¹ (100-140 GJ t_{NH3}⁻¹) using a DBD reactor and promoted Ru catalyst³⁸, but the challenges lie in the uncompetitive energy efficiency compared to commercial Haber Bosch (28-33 GJ t_{NH3}⁻¹) and NH₃ decomposition³⁹. Additionally, recent reports suggest a mechanocatalytic method of NH₃ synthesis under (near) ambient conditions^{40,41}, by ball-milling the catalysts under N₂ and subsequently introducing H₂, showing early promise of comparable energy efficiency to the Haber-Bosch⁴⁰.

Electrochemical oxidation of N₂ by electrolysis to fixate N₂ (N_{2(g)} + H_{2O(l)} + 2.5O_{2(g)} \rightleftharpoons 2HNO_{3(aq)}, $\Delta G^\circ = +87.7$ kJ/mol, eq. 5) expends much less energy than $\Delta G^\circ = +678.5$ kJ/mol for the reductive counterpart (eq. 3). Such processes can in principle replace the synthesis of NH₃ and subsequent oxidation of NH₃ by the Ostwald Process (2NH_{3(g)} + 4O_{2(g)} \rightleftharpoons 2HNO_{3(aq)} + 2H_{2O(l)}; $\Delta G^\circ = -590.8$ kJ/mol¹¹, eq. 6) for the production of nitric acid, a primary commodity chemical of oxidized N₂⁴². The remarkable difference in the energy expenditure for N₂ fixation between reduction and oxidation can be noted clearly by standard potentials of electrochemical half-cell reactions plotted on the standard hydrogen electrode (SHE) scale and also on the absolute electron energy scale referenced to the free electron in vacuum⁴³, as shown in Figure 2a. The standard potential for N₂ reduction (N_{2(g)} + 6H⁺ + 6e⁻ \rightarrow 2NH_{3(g)}, 0.06 V_{SHE}, -4.50 eV) is considerably higher than that of water splitting to generate O₂ (2H_{2O(l)} \rightarrow 4H⁺_(aq) + O_{2(g)} + 4e⁻, 1.23 V_{SHE}, -5.66 eV). The difference indicates the energy need of pumping electron energy from -5.66 eV to -4.50 eV for each electron

transferred, in agreement with standard reaction free energy of +678.5 kJ/mol for $\text{N}_{2(\text{g})} + 3\text{H}_2\text{O}_{(\text{l})} \rightleftharpoons 2\text{NH}_{3(\text{g})} + 1.5\text{O}_{2(\text{g})}$ (with 6 electrons transferred). On the other hand, standard potential for N_2 oxidation ($\text{N}_{2(\text{g})} + 6\text{H}_2\text{O}_{(\text{l})} \rightarrow 2\text{NO}_{3(\text{aq})}^- + 12\text{H}_{(\text{aq})}^+ + 10\text{e}^-$, 1.24 V_{SHE}, -5.68 eV) is very similar to that of water splitting to generate O_2 ($2\text{H}_2\text{O} \rightarrow 4\text{H}^+ + \text{O}_2 + 4\text{e}^-$, 1.23 V_{SHE}, -5.67 eV), where minimum energy is required to activate N_2 and H_2O to make NO_3^- from the thermodynamic standpoint.

The most technologically mature form of N_2 oxidation is the Birkland-Eyde process, where the reaction between N_2 and O_2 to form nitric oxide (NO) is assisted by electric arc-generated hot plasma^{44,45}. High-temperature thermal plasmas are not energy-competitive⁴⁶ and require rapid quenching to prevent NO decomposition back to N_2 ⁴⁷. Researchers are paying increasing attention to the use of warm and cold (non-thermal) plasmas, as its theoretical energy consumption⁴⁸ is more than twice lower than that from N_2 and CH_4 (eq. 3), yet a technological bottleneck lies in low conversion to product⁴⁹. More recently, a growing number of studies are dedicated to the electron and photon assisted conversion of N_2 to nitrate (NO_3^-)⁵⁰⁻⁵⁶ but seem to suffer significant kinetic limitations similar to the reductive counterpart.

[H2] Origin to N_2 activation challenges

Activating N_2 by reduction to make NH_3 is kinetically difficult, which demands much more energy than what is needed thermodynamically to drive reactions at high rates to make these processes economical. Catalyzing N_2 fixation has been limited largely by the cleavage of the $\text{N}\equiv\text{N}$ bond due to the inertness of N_2^2 , i.e. the high triple bond strength (9.79 eV), high ionization potential (15.84 eV), low electron affinity (-1.90 eV), and nonpolarity. Ru is considered the most active elemental heterogenous catalyst for thermochemical NH_3 synthesis (i.e. the Haber-Bosch process). The energetics of the possible elementary steps are examined. The free energy profile for an associative mechanism on Ru(0001) terrace, which involves N_2 bond cleavage via a hydrogenated intermediate (similar to nitrogenase⁶), is shown in Figure 2a. The protonation of adsorbed $^*\text{N}_2$ to $^*\text{N}_2\text{H}$ (step 1-2) has the largest thermodynamic barrier (1.02 eV). This is considered rate-limiting and prohibitively slow by invoking the Brønsted–Evans–Polanyi relationship⁵⁷, which linearly correlates the activation barriers to the reaction energies. In contrast Ru(0001) step sites adsorb N_2 more strongly than terrace sites and the thermodynamic barrier at the step sites for $^*\text{N}_2$ to $^*\text{N}_2\text{H}$ is much lower (~0.3 eV). In addition, the process can be understood commonly via a dissociative mechanism⁵⁸⁻⁶⁰, where N_2 is cleaved upon adsorption into atomic N, and then hydrogenated to release NH_3 . Although downhill in energy, the dissociation of N_2 to 2^*N has a significant activation barrier, and is revealed to occur only at step sites due to the prohibitively high activation barrier for N_2 dissociation on terrace sites^{61,62}. Experimentally, the activation barrier on a clean Ru(0001) single crystal (containing step site density of ~1%) is 0.4 eV and increases substantially to 1.3 eV when small amounts of Au, which preferentially decorate the steps, is introduced, thereby showing that the rate of N_2 dissociation is completely dominated by steps⁶². There are also significant uphill steps for the reduction of $^*\text{NH}_2$ to $\text{NH}_{3(\text{g})}$ (step 6-8) at the step sites on Ru(0001), signifying the cost of creating free sites. The apparent activation energy is the sum of both the activation energy of the rate-limiting step and the cost of making free sites in a non-trivial manner^{61,63}; this is the origin of the Sabatier principle.

Activating N_2 by oxidation is equally challenging, and very few systematic investigations on the oxidative N_2 fixation exist in literature^{67,68}. A reasonable starting point would be to consider a series of hydroxylation-deprotonation steps as computed for N_2 oxidation on rutile RuO_2 (110)⁵⁶ in Figure 2a, which shows N_2 activation is the most uphill step (1.86 eV), suggesting a substantial kinetic barrier for this reaction.

In interpreting free energy diagrams, an important distinction should be made between electrochemical and non-electrochemical steps. Electrochemical steps, such as those involving proton-electron transfers (i.e. all steps in Figure 2a except for N-N dissociation, adsorption and desorption), are affected by applied potential. The overpotential required to bring the most uphill electrochemical step downhill is plotted in Figure 2b (green) for associative N_2 reduction on transition metal terraces. In addition to the thermodynamic barrier, electrochemical steps can possess an additional barrier. For example, *Singh et al.* calculated the intrinsic electrochemical barrier (at $\Delta G_{step} = 0$) for the $^* \text{N} + \text{e}^- + \text{H}^+ \rightarrow ^* \text{NH}$ step on transition metal terraces to be 0.7 eV regardless of the free energy difference between the two states ($^* \text{N}$ and $^* \text{NH}$), and thus insensitive to the metal identity⁶⁶. We have used an intrinsic barrier of 0.7 eV for all proton-electron transfer steps in Figure 2a. Non-electrochemical steps, such as N-N dissociation (step 0-1 of the dissociative N_2 reduction, Figure 2a), adsorption (step 0-1 of the associative N_2 reduction/oxidation) and desorption (step 7-8 of N_2 reduction), are not affected by applied potential.

A feature of interest is the rate-limiting step, known as the maximum barrier along the reaction pathway whose rate is significantly slower than those of the other elementary steps, thus governing the rate of the overall reaction. The rate constant of the elementary step is given by $v \exp(-\Delta G^\ddagger/k_B T)$ from transition state theory, where the prefactor v equals $k_B T/h$ ($\sim 10^{13} \text{ s}^{-1}$ at 25 °C). The rate of reaction for heterogenous catalysis, expressed in $\text{mol cm}_{\text{cat}}^{-2} \text{ s}^{-1}$, is connected to the rate constant by multiplying with the concentrations of reactants if the first step is the rate limiting step, or by surface concentrations if the rate limiting step involves surface intermediates. This rate can be converted to the turnover frequency ($\text{mol site}^{-1} \text{ s}^{-1}$) by dividing the site area density of the catalyst ($\text{sites cm}^{-2}_{\text{cat}}$), to mass activity ($\text{mol g}_{\text{cat}}^{-1} \text{ s}^{-1}$) by multiplying the specific surface area ($\text{cm}^2_{\text{cat}}/\text{g}_{\text{cat}}$), and to geometric-area-normalized activity ($\text{mol cm}_{\text{geo}}^{-1} \text{ s}^{-1}$) by multiplying the roughness factor ($\text{cm}^2_{\text{cat}}/\text{cm}^2_{\text{geo}}$). To rationalize a catalyst's viability, one can calculate the rate constant to estimate the rate and establish the point at which the barrier becomes prohibitive.

In using the expression of $v \exp(-\Delta G^\ddagger/k_B T)$, we note that the errors due to the level of theory and a free energy correction of $\sim 0.25 \text{ eV}$ ^{67,68} correspond to ~ 5 orders of magnitude in rate. Generally, an active catalyst would have a turnover frequency greater than 1 s^{-1} , which corresponds to a barrier of 0.75 eV at room temperature. Therefore, free energy diagrams for electrochemical N_2 fixation under ambient conditions that involve an uphill step greater than 1.5 eV at the operating potential indicate non-viable catalysts, particularly if kinetic barriers have been neglected. However, a more quantitative and accurate description requires higher forms of simulation to capture the system's complexity, such as kinetic Monte Carlo simulation or microkinetic modelling; the latter shown in Figure 2b (red) for the thermochemical route of NH_3 synthesis. For the electrochemical route, we refer readers to ref⁶⁶ for the full microkinetic model.

The difficulty of finding catalysts with fast kinetics for N_2 fixation can be explained by the “scaling relations”⁶⁹, where the energetics of different elementary steps shown in Figure 2a cannot be controlled independently on a given surface. Such scaling relations can be manifested in the volcano dependence of catalytic activity on the adsorption energy of surface reaction intermediates. For example, the catalyst activity, computed via mean-field kinetic model of the dissociative mechanism, exhibits a volcano dependence on the N adsorption energy (Figure 2b, red)⁶⁹. On the right side of the volcano for weak-binding surfaces, N_2 dissociation is rate-limiting, while on the left side for strong-binding surfaces there is a low barrier for N_2 dissociation, but the surface is poisoned by N species. Fe, Ru and CoMo alloy exhibit the highest activity and further enhancement can be achieved by using alkali (electronic) promoters^{70,71}.

However, efficient, low-pressure Haber Bosch requires more active catalysts beyond the constraints set by the volcano⁷².

Scaling relations also constrain electrochemical N₂ reduction. The overpotential needed to have all the elementary reaction steps downhill for the associative mechanism (Figure 2b, green), exhibit a volcano relationship with the N binding energy on metal surfaces^{73,74}. More importantly, electrochemical N₂ reduction in aqueous electrolytes has to compete with electrochemical H₂ evolution as both reactions have similar standard potentials and electron energy on the absolute energy scale (Figure 2a). Unfortunately, the kinetics of water reduction to produce H₂ is much faster than that reduction of N₂ to NH₃, as seen in the comparatively lower overpotential for H₂ evolution (Figure 2b), translating to many orders of magnitude difference in the estimated rate (Figure 2b, green). In addition, the bond strength of any given metal surface to H (a sole intermediate of H₂ evolution) is stronger and linearly correlates with N-containing intermediates of N₂ reduction³³, indicates that the surface will be poisoned by *H⁷⁵, likely responsible for negligible NH₃ reported in aqueous systems^{76,77}. A study on wider N₂ electrooxidation trends are unavailable, but we expect a similar scaling relation between the reactant activation and subsequent hydroxylation or desorption steps, and scaling with *O₂ intermediates of the competing O₂ evolution.

Alternative strategies have been explored to overcome the activity and selectivity challenges in N₂ reduction. In thermochemical NH₃ catalysis, Chen *et al.* have demonstrated excellent activities using transition metal-LiH composite catalysts, where two active centers are present; transition metal sites to cleave the N₂ bond, and LiH to aid N hydrogenation and subsequent NH₃ desorption⁷⁸. In electrochemical NH₃ synthesis, the lithium-mediated approach has emerged, where the N₂ reacts with metallic Li to form Li₃N, followed by nitride protonation to evolve NH₃, including continuous lithium-mediated N₂ reduction in non-aqueous solvents⁷⁹⁻⁸² or a lithium-nitride cycling scheme^{83,84} (Figure S2, see Supplementary Information). The Li-mediated approach has decoupled reactant activation and subsequent protonation steps, where the non-aqueous solvents and the *in situ* formation of protective solid-electrolyte-interphase (SEI) layer restrict proton availability to the active site^{82,83}, potentially responsible for the high yields.

[H2] The need for a strict protocol

Progress in (photo)electrochemical N₂ fixation can benefit from developing a more rigorous protocol of measurements and product quantification, as state-of-the-art yields of NH₃ (and NO₃⁻) from these processes are significantly lower than thermochemical NH₃ production (see Results.) while contamination (possible sources summarized in Table 1) can be present at similar or greater concentration levels than the measured product⁷⁶. In addition, the NH₃ yields for low-temperature and/or low-pressure thermal catalysis exponentially drops, and accurate activity measurements can suffer from adventitious N contamination, N and/or H leaching, and non-catalytic NH₃ generation⁸⁵, where such uncertainties in catalytic activity measurements can propagate into subsequent kinetic analyses.

The field has been plagued with false positives. The first observation of electrochemical N₂ fixation was in 1807 by Sir Humphry Davy, who reported production of NH₃ and HNO₃ by passing current through distilled water⁸⁶, but was proven non-reproducible some 90 years later⁸⁷. In 1995, Boucher *et al.* demonstrated inability to reproduce reported photochemical NH₃ synthesis using TiO₂ under rigorous measurements⁸⁸. More recently, Shipman *et al.* retested Sn(II) phthalocyanine catalysts in 2017 for electrochemical N₂ reduction, concluding that the NH₃ measured arose from decomposition of their catalyst⁸⁹. Litch *et al.* retracted their work on nanoscale Fe₂O₃ in molten hydroxide from *Science* in 2020, citing adventitious NH₃

synthesis from trace NO_x^- contaminants in their electrode material. MacFarlane, Simonov, and coworkers retested and reported no electrochemical activity for VN⁹⁰, and Bi and Au catalysts⁹¹, reported previously to have high activity^{92–94}, after accounting for N leaching from the VN catalyst and properly cleaning the supplied N_2 gas for NH_3 and NO_x impurities.

The ubiquity of contamination sources calls for an exceptional scrutiny. In this Primer, we introduce a general protocol focused on confirming genuine activation of inert N_2 and elaborate details in performing catalytic measurements (Experimentation). We then evaluate state-of-the-art results, primarily focused on (photo)electrochemical and thermochemical systems using the protocol's framework and discuss best practices in reporting and interpreting both experimental and DFT data (Results). The potential uses of these N_2 activation reactions is discussed in the context of current practices, highlighting the importance of research in these areas (Applications), and we explore factors affecting reproducibility, thereby establishing reporting standards (Reproducibility and Data Deposition). Finally, we discuss ways to overcome cost-limitations of performing repeated isotope-labelled experiments (Limitations and Optimizations) and outline future directions in N_2 catalysis research including community-wide adoption of rigorous protocol, in situ measurements for mechanistic understanding and field-specific needs (Outlook).

[H1] Experimentation

A general protocol for carrying out electrochemical, photo(electro)chemical, and thermochemical N_2 activation experiments is presented, which can be extended to apply across all N_2 activation fields. This is followed by an in-depth discussion of the experimental setups and necessary measurements, and various different methods of product detections to determine successful product synthesis.

[H2] General protocol for N_2 reduction and oxidation reactions

We propose a general protocol shown in Figure 3, to holistically account for various contamination sources, applicable to any N_2 activation reactions, which is based on the principle that one should always be wary of contamination.

The first step involves the experiment setup and it is run with N_2 . If no product is measured, re-iterations with new parameters or catalysts is necessary, until the desired product is detected. Next, one must measure or estimate the total equivalent N mass of the system, $mass_{sys}$, to account for possible contamination sources, which includes $mass_{N,cat}$, $mass_{N,electrolyte}$, $mass_{N,absorber}$ and $mass_{N,gas}$. Precise definitions of these terms are outlined in Box 1.

For successful synthesis, the amount of N in the product measured must exceed the amount of N in $mass_{sys}$ by a factor of 2 ($mass_{prod} > 2 mass_{sys}$) to account for unexpected sources of contamination, and one must in this case ensure that $mass_{prod}$ is well above $mass_{N,cat}$. The product concentration (C_{prod}) in the electrolyte or gas stream must be higher than 100 ppm, based on olfactory detection of NH_3 , to exclude unaccounted sources of contamination (e.g. glassware, breath, laboratory air, etc.), as the reported yield above 100 ppm would easily be detectable by olfaction⁹⁵, and far greater than common source of contamination in the lab.

If both these criteria are met, repeated testing is necessary with independently prepared samples to confirm reproducibility. If these criteria were not met, the measured yield of product might stem from contamination, and further evidence of successful synthesis via quantifiable isotope-labelling experiments is necessary. First, one must test using an inert gas (e.g. Ar or pure H_2) and N_2 in the absence of driving

force. These conditions can range from operating an open circuit potential for electrochemical systems, under dark illumination for photo(electro)chemical systems, or without applied heat for thermochemical systems, which is essential to account for sources of contamination in the experimental set-up, as this should give no or significantly less product compared to N₂ with a driving force. Repeated identical testing of independently prepared batches follows, to ascertain reproducibility, and determine the level of inherent contamination in the system (if any). Additionally, a stability test is needed to eliminate the possibility of non-catalytic generation of the product, such as N-leaching from an N-containing catalyst. Once all sources of contamination were accounted for, quantitative isotopic labelling experiments is necessary. In detecting the product, two separate quantification techniques must be used, where at least one of them is isotopically sensitive, and these two methods must show repeated and reproducible overlap between the use of ¹⁴N₂ and ¹⁵N₂ over multiple points (see Results). It is important to include a proper gas cleaning procedure, as isotope labelled ¹⁵N₂ gas can contain significant amounts of NO_x and NH₃ impurities⁹⁶.

In thermal catalysis, kinetics parameters, such as activation energy and reaction orders in the kinetic regime, are a key metric to report. It is important that the kinetics measurements are carried out far from the equilibrium to avoid the reaction reversing, where mass and heat transfer limitations are minimized. Kinetic measurements to extract activation energy and reaction orders are extremely beneficial for elucidating the reaction mechanism. In particular, the effect of NH₃ concentration on the reaction orders and the apparent activation energy must be accounted for (see Results). Electrochemical and photo(electro)chemical systems can also benefit from kinetic measurements, although this is not common in the literature. These measurements are difficult to obtain, as reliable determination of the partial current density toward NH₃ for a given system might be highly inaccurate, due to a historic contamination issues in the field. With rigorous experimentation, measuring parameters such as the pH dependence of the N₂ reduction activity might provide insights on the reaction path and mechanism⁹⁷. The only published and proven work reporting kinetic measurements have investigated the effect of proton and N₂ concentration and their respective reaction orders in the lithium-mediated system⁸¹. In addition, Tafel analysis can be a powerful tool for elucidating rate determining steps, but overly simplified assumptions will lead to inaccurate description of the electrocatalysis⁹⁸, and researchers should apply caution when interpreting Tafel slopes as they may contain many artefacts⁹⁹. Furthermore, when including kinetic measurements, great care should be taken with reporting a clear definition of the kinetic parameters and kinetic models used¹⁰⁰.

[H2] Experimental setup

[H3] Electrochemical measurements

Electrochemical measurements are typically conducted in a cell setup as depicted in Figure 4a, into which gas streams are introduced. As feed gases (Ar, ¹⁴N₂, and ¹⁵N₂) can contain significant amounts of activated N-species (such as NH₃, NO_x and N₂O) as contaminants^{96,101}, the gas must be cleaned prior to use, using a reduced Cu catalyst and freeze trap⁷⁶ or commercial gas purifiers. One can also chose to not clean the gas, but measure all the N-containing contaminants, and include them in the value for $mass_{N,gas}$. In the electrochemical cell, depending on the desired reaction, the working electrode (WE) will either facilitate N₂ reduction or oxidation, while the counter electrode (CE) runs the respective counter reaction, and the reference electrode (RE) determines the potential at the surface of both other electrodes. In aqueous electrolytes, numerous commercial REs are available¹⁰² and should be calibrated against the reversible hydrogen electrode (RHE) by measuring the equilibrium potential for H₂ oxidation and evolution on a Pt electrode. Alternatively, a well-known RE such as saturated calomel electrode (SCE) in aqueous electrolytes, or Li in non-aqueous electrolytes can be utilized, with a conversion to RHE. Calibrating the RHE in non-aqueous electrolytes can be challenging¹⁰³, but is possible, since the H₂ oxidation and evolution

potential is measurable for lithium-mediated N₂ reduction⁸⁰. When measuring N₂ reduction in non-aqueous electrolytes, researchers can use the same REs as those used in the battery literature, such as metallic Li¹⁰⁴, and calibrate the RE to the RHE scale in their electrolyte of choice in a separate measurement.

As activated N-species is ubiquitous in the environment, electrochemical and photo(electro)chemical systems are prone to contamination. Possible sources of contamination are shown in Table 1, along with a recommended method of elimination. Specifically, the commonly used Nafion membrane has been shown to contaminate the setup^{76,105,106} and degrade in the presence of NH₃^{107,108}, so extra care must be taken if using this membrane. Control experiments, such as testing using Ar with a driving force and N₂ without a driving force with time-dependent experiments, are needed. All adventitious sources of activated N₂ can be avoided by the use of purified isotopically labelled ¹⁵N₂, and the subsequent measurement of ¹⁵NH₃ or ¹⁵NO_x by an isotope sensitive method^{76,77}. Liquid samples from the electrolyte should be investigated, repeated for reproducibility, and quantified via at least two separate methods, and the yield produced using ¹⁵N₂ must be comparable to the yield measured with ¹⁴N₂.

Chronopotentiometric (CP) and/or chronoamperometric (CA) measurements show the stability of the system over time, and representative data for these should be reported, with a description of whether Ohmic correction is utilized. Once the synthesized product is detected (see Experimentation), the product yield and Faradaic efficiency can be calculated as a function of potential vs RHE, enabling the determination of the optimum for each of these factors in the system. Moreover, the difference between the operating potential and the equilibrium voltage approximates the overpotential, a critical figure-of-merit. The overpotential for N₂ reduction to NH_{3(g)} is pH and electrolyte independent. The Nernstian shift in the equilibrium potential occurs due to a change in product and reagent concentrations that affect the overall pH of the solution, and can be taken into account via the actual amount of NH₃ produced. Relative to standard conditions, the equilibrium concentration of NH_{3(aq)} or NH_{4⁺(aq)} can be determined by thermodynamic data (solvation energy) or measured directly via NMR¹⁰⁹. At pH = 0 the difference between the standard equilibrium potential N_{2(g)}/NH_{4⁺(aq)} is 0.27 V vs RHE, while at pH = 14 the standard equilibrium potential of N_{2(g)}/NH_{3(aq)} is ~0.1 V vs RHE¹¹. However, this Nernstian shift is insignificant when there is a large overpotential for N₂ reduction, such as the case of non-aqueous lithium-mediated NH₃ synthesis.

[H3] Thermochemical measurements

Thermochemical measurements are usually conducted in a fixed-bed flow system as shown in Figure 4b, where the catalyst is loaded into the reactor and pretreated under specified conditions. The reactant gases (N₂ and H₂) are passed over the catalyst bed with a certain space velocity, where the reaction rates are not limited by gas transport. The reactant gases may need purification by in-line gas purifiers to reduce the content of impurities (e.g. H₂O, O₂, CO₂) to ppt-level, as these might affect the surface of the active catalyst e.g. via poisoning. The measurements should be conducted under steady-state conditions as a function of temperature and pressure. The produced NH₃ is typically trapped in a downstream diluted sulfuric acid solution, which is then quantified by using ion chromatography or a conductivity meter (see Experimentation). Once the amount of produced NH₃ is determined, the related kinetic parameters (e.g., NH₃ synthesis rate and yield) can be obtained.

Reactors made of stainless steel are commonly employed for pressurized reactions. Transition metals (e.g. Fe, Cr, Ni) in the reactor may not be inert, and could interfere in the NH₃ synthesis through interacting with the catalyst. It is recommended to use a reactor made of, or lined with, inert material such as quartz to

exclude the contribution of a “reactive reactor”¹¹⁰. A blank test (without catalyst loading) should be performed prior to catalyst evaluation, to make sure there is no detectable NH₃ contamination present in the system. In addition, benchmark catalysts, such as Cs-promoted Ru/MgO should be prepared and tested, with an activity comparable to that previously reported (Cs–Ru/MgO with 3–6 wt.% Ru loading should have an NH₃ formation rate from 8–14 mmol g_{cat}⁻¹ h⁻¹ at 400 °C and 10 bar)^{111–113}. These two experiments are important for validating the testing system.

[H2] Product detection and Isotope Labelling

[H3] Non-isotopic product detection

UV-Vis spectroscopy allows the fast and easy quantification of NH₃ through the colorimetric reactions of either indophenol blue or Nessler’s reagents, with a limit of detection down to 10 ppb (~0.5 μM) NH₃ (Figure 5 a, b). The method induces a chemical reaction between NH₃ and the reagents of choice, leading to the formation of a colorful dye that is quantifiable via UV-vis spectroscopy with a peak value at 625 nm for indophenol blue and 425 nm for Nessler’s reagents¹¹⁴. Despite the simplicity of these techniques, interferences in the chemical reaction forming the colorful dye may be caused by the presence of different ions in the media (Fe³⁺, Co²⁺ to S²⁻, etc.), the reaction time, and diverse pH conditions, which may impede accurate quantification of NH₃¹¹⁵. Nevertheless, some of these can be overcome by e.g. utilizing Seignette reagent (also known as Rochelle salt), which allows the analysis of samples with high salinity¹¹⁶. The salicylate method (similar in principle to indophenol) is also commonly used to detect NH₃. Recently, Giner-Sanz *et al.* show a convenient methodology to correct the effect of strong Fe III interference by using an interference model requiring only three experimental curves¹¹⁷.

The Griess assay is widely adopted for the quantification of NO₂⁻. To quantify NO₃⁻, the sample can be reduced to NO₂⁻ using Zn powder¹¹⁸. However, the Griess method suffers from a comparatively high limit of detection of 500 ppb (~10 μM), and interferences with Fe³⁺, Cu²⁺, S²⁻ or I⁻, and should be used with caution.

Conductivity meter provides a facile and widely adapted method in thermochemical reactions for quantifying NH₃ in a limit of detection of 1 ppm (Figure 5a, c). The concentration of NH₃ from the outlet gas trapped in a diluted sulfuric acid solution can be determined by measuring the decrease in ion conductivity (corresponding to the conversion of H⁺ to NH₄⁺) of the solution. A correlation/calibration curve of the change of conductivity and the amount of NH₃ produced should be determined under a given temperature and concentration of the solution. As both of these parameters have strong influences on the ion conductivity in the solution¹¹⁹, it is important to maintain a constant temperature and concentration of the solution in each measurement.

[H3] Isotopic Product detection

Nuclear Magnetic Resonance (NMR) is a useful technique for determining the chemical composition of a sample, and can accurately detect NH₃ down to 50 ppb (~3 μM), as shown in Figure 5a, d. It utilizes the magnetic properties of nuclei with non-zero spin and non-zero magnetic dipole moment. The sample composition can be determined based on the characteristic radio frequency (RF) pulse required for the excitation of the nuclei¹²⁰. As the area of the signal is proportional to the number of nuclei affected by the applied RF pulse, the concentration of the sample can be inferred based on calibration curves. ¹H NMR can be used to differentiate isotopes of ¹⁴NH₃ and ¹⁵NH₃. Due to the difference in spin between ¹⁴N and ¹⁵N, the scalar interaction of ¹H will lead to respectively a triplet peak with a characteristic spacing of 52 Hz, and a

doublet peak with a splitting of 73 Hz. For non-aqueous systems, the use of organic solvents might interfere with the detection of the NH_3 signal, however, different methods for solvent signal suppression are reported in the literature^{76,121}.

The quantification of $^{14}\text{NO}_3^-$ and $^{15}\text{NO}_3^-$ can be performed using N-NMR, but the low production yield of the experiment, coupled with the unfavorable NMR properties of ^{15}N (i.e. low gyromagnetic ratio and long T1 relaxation constants)¹²², implies that long-duration electrochemical experiments must be performed to allow reproducible quantification at multiple points. One study covering N_2 oxidation has used ^{15}N -NMR⁵⁶, requiring >100 ppm concentration of NO_3^- for detection, which was achieved via a 50 hour experiment. Finding a more convenient isotopic NO_3^- detection method is therefore a gap that must be addressed to enable development in the field of electrochemical N_2 oxidation.

[H1] Results

A state-of-the-art overview of the electrochemical, photo(electro)chemical, and thermochemical N_2 activation fields is presented, applying the protocol from the Experimentation section to determine levels of contamination. Important reporting metrics and issues hindering progress in the field is covered in this section, along with interpretation of both experimental and density functional theory results.

[H2] Evaluation of N_2 Catalysis Experiments

Figure 6a depicts the yields of the product ($mass_{prod}$), namely NH_3 for N_2 reduction and NO_3^- for N_2 oxidation, relative to the size of the system from which N-contaminants may originate ($mass_{sys}$). Thermochemical systems typically produce several orders of magnitude more NH_3 (especially at temperatures >300 °C) compared to $mass_{sys}$. As a result, these systems can cross the $mass_{prod} > 2 mass_{sys}$ line within the first few hours of experimentation, and have experimental durations upwards to 100 hours. (See Supplementary Information for a demonstration) The ease with which thermochemical experiments surpass the size of the system explains why contamination issues are not typically prevalent in thermal catalysis, and also inherently points towards an intrinsically high catalyst activity.

In contrast, electrochemical, photochemical, and photoelectrochemical experiments typically show yields of NH_3 or NO_3^- in orders of magnitude less than the size of the system. None of these catalytic systems fulfill the $mass_{prod} > 2 mass_{sys}$, and would require several orders of magnitude longer experimentation (with proper gas cleaning) to produce more product, and thereby move vertically up to cross the criteria of $mass_{prod} > 2 mass_{sys}$. We note some suspiciously high reported yield rates from recent (photo)electrochemical studies (Figure 6d), including the Bi point⁹⁴ operating at only -0.7 V_{RHE} which reported higher production rates than some highly active thermochemical catalysts operating at elevated pressure and temperature conditions. This should have raised some concerns due to the high computed barrier in the same paper (>2 eV) and the selectivity challenge against H_2 evolution (See Figure 2a). As the flagged point has been shown as non-reproducible⁹¹, this example serves to highlight how adventitious N sources can lead to non-genuine N_2 fixation and inflate the reported yield rates in literature. Comparison of the reported intrinsic activity i.e. turnover frequency with thermochemical catalysts also shows this conclusion (see Figure S3 in Supplementary Information) and can be used to screen potential false positives. In most cases, the catalytic activity of electro/photocatalysts are much lower than the thermal counterpart and thus require hundreds of hours of experimentation to surpass the $mass_{sys}$ (see Supplementary Information for demonstration). Therefore, quantitative isotope-labelling experiments, along with a proper gas-cleaning protocol, is a convenient and unambiguous way to verify genuine N_2 fixation, thereby proving the origin of the activated N.

As of now, non-aqueous electrolytes are the only known conditions in which genuine electrochemical N₂ reduction under standard temperature and pressure is reliably demonstrated^{76,81,82}. Several generations of breakthroughs are still needed to enhance reaction kinetics and achieve viable photo- and (photo)electrocatalytic performances for commercial application¹²³. Advances in catalyst and electrolyte design are therefore required¹²⁴, but low concentrations of *mass_{prod}*^{76,125} in these fields means a rigorous experimental protocol must be followed to ensure the integrity of reported experimental results.

The current goal in thermochemical NH₃ production is to decrease the temperature and pressure, enabling milder operational conditions compared to current Haber-Bosch plants²⁹. However, lowering the temperature leads to an exponential decrease in the formation rate, which increases the possibility of contamination, particularly if the catalyst contains activated N. The *mass_{prod}* for these low-temperature systems also becomes so low, that they fall below the *mass_{prod}* > 2 *mass_{sjs}* threshold and are comparable to some of the more active electrochemical systems, necessitating isotope measurements. We note that the integrity of the reported formation rate must be rigorously evaluated especially at the low production points, because if the activity measurement is based on incorrect yields of NH₃, the error will propagate to the subsequent kinetic analysis.

[H2] Electrochemical and Photo(electro)chemical N₂ Reduction and Oxidation

[H3] Reporting metrics of experimental results

To measure the catalytic performance, CA and/or CP measurements are carried out, the product concentration determined, enabling a calculation of the yield and Faradic efficiency of the process. Typically a metric such as the partial current density or formation rate is plotted as a function of applied current or potential, and the Faradaic efficiency is overlaid on a separate y-axes, displaying the maximum performance of the system (Figure 7a)⁷⁹. In photoelectrochemical systems, incident photon-to-current efficiency should be calculated utilizing a monochromatic light source¹²⁶. All experiments should be repeated several times, from at least three independent batches of experiments to allow appropriate determination of a mean and its associate standard deviation. Representative CA or CP graphs should also be shown, as this illustrates the catalyst stability with time (Figure 7b). In the case of powder photocatalysis, the amount of product formed should be plotted versus time, and a production value per hour and gram catalyst can be extracted. The amount of product formed must be correlated with the amount of incident photons reaching the reaction vessel by calculating the average quantum yield (or quantum efficiency), which is measured with monochromatic light sources or cut-off filters at a given wavelength^{127,128}.

As rigorous product detection is key to appropriately evaluating activity of (photo)electrochemical catalysts, product concentrations should be verified using at least two independent detection methods, and must show quantitative agreement with each other over multiple points¹²⁹. Typically, this is shown by comparing results from colorimetric methods with results from isotope labelled experiments⁷⁶. This should demonstrate that the amount of product measured using appropriately cleaned ¹⁵N₂ (seen in Figure 7c) can reproduce quantitatively the amount measured using ¹⁴N₂ over numerous points, as shown in Figure 7d, and that there is a linear increase in detected product as a function of time or charge passed.

[H3] Issues hindering progress in (photo)electrochemical N₂ activation

Due to the selectivity challenge and the activity issue, reported yields and Faradaic efficiencies are very low, both for electrochemical N₂ reduction and oxidation. The reported partial current densities towards NH₃ are <~1 mA/cm_{geo}² with reported Faradaic efficiency up to 60%. However, NH₃ is ubiquitous in the environment¹³⁰ in concentrations similar to or greater than those reported, so great care must be taken with

experimentation to avoid false positives. Many reports in Figure 6b now include isotopic labelling experimentation (crossed points), which is a shift towards utilizing isotopes that has occurred over the previous 2 years⁷⁶. Unfortunately, many of the reports only do isotopic labeling of a single experiment^{94,131–137}, which does not demonstrate reproducibility, as this is not enough to prove beyond doubt that synthesis of the product takes place. Also, the isotopically labelled gas typically contains ¹⁵NH₃ and ¹⁵NO_x impurities⁹⁶, and most of these new reports do not clean the gas prior to measurements, or clean it incorrectly¹⁰¹. Many of these reports are aqueous systems (non-stared), which typically suffer from low selectivity due to the competing H₂ evolution reaction³³, and could therefore easily be contaminated. The flagged Bi report⁹⁴ demonstrates the possibility of inflated yield rates due to contamination: we therefore urge researchers to reexamine high catalytic activity results via a rigorous experimentation^{76,101} (see Experimentation). The Li-mediated system (denoted Li_xN/xx) was initially discovered by Tsuneto *et al.*^{138,139}, and has recently gained renewed interest, as it has been proven to work via rigorous isotope sensitive experimentation⁷⁶. This system is displaying comparatively increased partial current density towards NH₃⁸¹, however, it requires very negative potentials, due to the necessity of Li plating, making it energy inefficient.

For N₂ oxidation (squares, Figure 6b), the partial current densities to NO₃[–] are less than ~10 $\mu\text{A}/\text{cm}^2_{\text{geo}}$ ⁵⁰, and the highest activity catalysts tend to correspond to Faradaic efficiencies <~1%^{56,140}. The field of electrochemical N₂ oxidation is novel and small, with only a handful of published papers^{50–52,56,140}. However, there is hope of a significant increase in the selectivity, as H₂ evolution is not a competing reaction to N₂ oxidation, as it is with N₂ reduction. More theory to elucidate the reaction mechanisms is needed, along with a standardization and rigor regarding measurement, as the yields and product concentrations are still very low.

In the case of photon-driven N₂ fixation, there is a general lack of rigorous testing¹¹⁵. Hirakawa *et al.* showed that activity of titania is highly dependent on supplier, a fact that has been attributed to differences in oxygen vacancy abundance¹⁴¹ or carbon contaminants¹⁴². Nonetheless, reports of photochemical N₂ fixation on titania and numerous other materials have been growing exponentially^{64,115}. Literature results in photochemical N₂ fixation must be viewed in the context of experimental rigor, which includes not only mere isotope labelling experiments but also tangible efforts to account for contamination sources including the elimination of ¹⁵NH₃ and ¹⁵NO_x impurities in gas streams. The necessity of isotope-labelled experiments is due to the inherent measurement challenges similar to those within electrochemical systems. For instance, some of the most widely utilized semiconductor photocatalysts for N₂ reduction are based in carbon nitride materials^{143,144}, which display plenty of amine terminal moieties and a general high N content that can lead to meaningful amounts of NH₃ upon degradation¹⁴⁵. Additionally, residual alcohols, amines, organic solvents can interfere with NH₃ quantification which lead to unreliable determination of NH₃ yields^{115,146}. Thus far, we are not aware of any photochemical studies in which isotope labelling shows quantitative agreement between ¹⁴N₂ and ¹⁵N₂ over multiple points (i.e. as a function of illumination time), along with proper gas cleaning to scrub away ¹⁵NH₃ and ¹⁵NO_x impurities. Nonetheless, theoretical works suggest that photo-excited holes or electrons may facilitate N fixation more easily than metal electrodes, as the adsorbates at the electrodes may not be in equilibrium with the charge carriers³³.

[H2] Thermochemical N₂ Reduction

[H3] Reporting metrics of experimental results

To evaluate a catalyst, the effects of temperature, pressure, and space velocity on catalytic activity as well as stability testing should be done. The typical reports of catalytic performance are shown in Figure 8. A temperature-dependent activity test within a certain temperature range (e.g. 250-400 °C) should be conducted, and a benchmark catalyst (Cs-Ru/MgO) should also be tested under identical condition. Special care should be given to the measurement of low-temperature activity (temperatures below 250 °C). For some of N-containing catalysts, such as nitrides, amides, imides and N-doped carbonaceous support, the catalysts should be reduced/pretreated under H₂ or H₂/N₂ at elevated temperature long enough to remove any reactive species from the catalyst. The stability is also crucial for evaluating the performance of a catalyst, and the activity data is meaningful only if there is stable performance. A life-time evaluation should show NH₃ production that is greater than the amount of N in the system, moreover, NH₃ concentration in the outlet gas should be greater than 100 ppm. Otherwise, isotope sensitive measurements are necessary.

Kinetic measurement should be conducted under conditions far from the thermodynamic equilibrium and in the absence of mass and heat transfer limitations (Figure 8c). From the power-law rate equation, $r = kP^{\alpha}_{NH_3}P^{\beta}_{N_2}P^{\gamma}_{H_2}$, where r is the reaction rate, k is the rate constant, P is the partial pressure of the reactants or product, α , β , and γ are the reaction orders with respect to NH₃, N₂, and H₂,^{147,148} the reaction rate is affected by the partial pressures of all gaseous components (N₂, H₂ and NH₃). The reaction order of NH₃ (α) should be measured by changing the flow rate (F) of reactant gas while keeping the N₂ and H₂ partial pressure constant. The reaction order of NH₃ (α) could be obtained by plotting $\log(P_{NH_3})$ (or $\log(C_{NH_3})$, C_{NH_3} is the NH₃ outlet concentration) vs. $\log(I/F)$. The reaction order of N₂ (β) should be determined by plotting $\log(r) - \gamma\log(P_{H_2}) - \alpha\log(P_{NH_3})$ vs. $\log(P_{N_2})$. Because the partial pressure of H₂ will not change significantly during catalytic testing, $\gamma\log(P_{H_2})$ can be regarded as a constant. The β could be obtained by plotting $\log(r) - \alpha\log(P_{NH_3})$ vs. $\log(P_{N_2})$ (Figure 8b). However, the term $\alpha\log(P_{NH_3})$ should not be omitted unless α is close to zero or NH₃ partial pressure is kept constant. Only under such circumstance can β be obtained by directly plotting $\log(r)$ vs. $\log(P_{N_2})$. The similar method is applied when determining γ . Calculating this result without keeping the NH₃ partial pressure constant may lead to a problematic interpretation of the reaction mechanism.

Generally, the N₂ order is positive and close to unity for the conventional oxide or carbon supported catalyst because the rate-determining step of these catalysts is the N₂ activation. However, H₂ and NH₃ orders can differ for various catalysts. For the iron-based catalysts, the H₂ order is positive and the NH₃ order is negative because of the strong adsorption of N^{149,150}. For some of the Ru-based catalysts, the H₂ order can be negative, due to being strongly inhibited by hydrogen¹⁵¹.

The apparent activation energy (E_a), in theory, should be determined by plotting $\ln(k)$ vs. $1/T$, rather than $\ln(r)$ vs. $1/T$, mainly because the variation of NH₃ partial pressure has influence on the reaction rate according to the power-law rate equation. Thus, E_a should be measured at a constant NH₃ pressure. As shown in Figure 8d, the apparent E_a calculated at constant NH₃ pressure were greater than those determined at constant flow rate over RuCl₃/γ-Al₂O₃ catalysts¹⁵². Thus, the importance of NH₃ partial pressure should be considered in the kinetic measurements, as it could otherwise lead to inaccurate values.

[H3] Issues hindering progress in thermochemical N₂ reduction

Generally, catalysts operated at lower temperature are associated with a lower NH₃ synthesis rate. More recently, reactive catalytic materials have been employed for thermal NH₃ synthesis (Figure 6c). Some of

the materials such as electrides¹¹¹, hydrides⁷⁸, nitrides¹⁵³, and oxy-hydrides¹⁵⁴ have been found effective in promoting/synergizing with transition metals, making early- and/or late-transition metals highly active. Some of the transition metal hydrides alone were also found to be catalytic active^{155,156}. Those materials, however, have dynamic responses to the reacting environment. A recent neutron scattering investigation reveals formation of H-containing species in the C12A7:e⁻ lattice under reaction conditions¹⁵⁷. The TiH₂ shows the potential nitridation of the surface during the reaction¹⁵⁵. The VH_{0.39} is most likely converted into VH_{0.44}N_{0.16} under reaction conditions, which is the stable active composition¹⁵⁶. Amides, hydrides and nitrides of alkali/alkaline earth/rare earth metals can also react with H₂, N₂ and/or NH₃¹⁵⁸. Moreover, catalyst made of coordination-unsaturated transition metal atoms or clusters may alter its chemical composition or physical state in response to the reacting environment. Characterization on a catalyst quenched from reaction would be more meaningful to provide information on the composition and chemical state of active phase/site. However, this has yet to be fully addressed.

Adventitious N source can also be significant when claiming catalytic activity with NH₃ concentration below 100 ppm or $mass_{prod} < 2 mass_{sys}$. In addition to the possible sources of contamination discussed in electrochemical N₂ reduction/oxidation reactions, attention should also be given to reactive catalysts that would build up lattice or surface N species *in situ* under N₂- or NH₃-rich atmosphere and elevated temperatures. Those N species have a chance to convert to NH₃ in a non-catalytic way when reaction condition allows (e.g., H₂-rich environment or low temperature), which may result in a false-positive, thus calling for verification via isotope labelling in the activity test as suggested.

[H2] Reporting and interpreting density functional theory results

Quantum mechanical simulations, typically based on density functional theory (DFT), are useful in understanding the mechanisms of N₂ activation. In this section, best practices in creating free energy diagrams, assessing active site stability, and rationalizing free energy diagrams are discussed.

[H3] Creating free energy diagrams

When creating free energy diagrams, it is critical to ensure that the initial and final states correspond to gas-phase N₂ and gas-phase/aqueous products respectively (for liquid-phase systems vapor pressure of N₂ can be used) so the overall reaction energy is independent of the catalytic material. For electrochemical free energy diagrams, a convenient model of applied potential is the computational hydrogen electrode (CHE) model¹⁵⁹, but more sophisticated models of applied potential may provide more accurate energies^{160,161}.

Considering the free energy of species, rather than just the energy obtained directly from DFT, is critical whenever computed energies are compared to experimental values¹⁶². At 0 K, the free energy consists of the energy obtained from DFT and the zero point energy. The temperature-dependent free energy includes additional contributions from enthalpy and entropy, which can be computed through statistical mechanics (we refer the readers consult standard DFT textbook¹⁶³ for how each term is calculated). As an approximate upper bound, the entropy can be computed by assuming the adsorbate acts as a harmonic oscillator, which can lead to over-estimation in the case of low-frequency modes since the entropy diverges as frequency goes to zero for a harmonic oscillator, calling the need of rigorous treating and reporting of low-frequency modes¹⁶⁴. Compared to the DFT energies, the inclusion of all free energy terms generally causes surface states to be less favorable due to the vibrational energy of the adsorbed states and the loss of entropy as they are bound to the surface. For example, the *N₂H surface species gains 0.16 eV to be adsorbed on Ru (211) when considering only the DFT energy (Figure 9a orange). However, it is destabilized by 0.67 eV

due to the entropy loss relative to the gas phase and by 0.16 eV due to changes in the zero-point energy of the bonds, leading to an energy penalty of +0.62 eV for adsorption (Figure 9a black). This increase reveals that not considering the relevant free energy can lead to qualitatively incorrect conclusions of thermodynamic driving force for elementary reaction steps and what the rate-limiting steps are.

[H3] Assessing Active Site Stability

The feasibility of an active site model can be assessed in terms of at least two criteria: stability and reactivity. An active site's stability should be assessed by computing its surface energy using ab initio thermodynamics¹⁵⁹. In general, activity and reactivity are related by a non-linear "volcano plot" relationship and sites that are more reactive tend to be less stable. Therefore, it is necessary to find a trade-off between reactivity and stability^{165,166}. Figure 9b shows an example of an activity-stability plot for surfaces toward O₂ reduction reaction on a number of Pt (111)-derived surfaces, where predicted current density represents activity and surface energy represents stability. The most relevant surfaces form a Pareto-optimal frontier along the activity/stability axes. Surfaces on the Pareto-optimal line represent optimal trade-offs between activity and stability, whereas surfaces below the line are sub-optimal. Surfaces further to the right are less stable and thus more challenging to generate under the atmospheric conditions used as the reference state. However, the stoichiometry active sites can vary, and their relative stability will vary depending on the chemical potential of the environment. Therefore, it is critical to consider the relevant chemical potentials when assessing active site stability. Competitive adsorption is also an important component of active site stability. For example, analysis of N₂ adsorption free energy often assumes that there is no competitive adsorption from abundant spectator species such as H*, which may prohibit adsorption and reaction⁷³. Surface phase diagrams provide a useful tool to assess stability and coverage of competing intermediates as a function of chemical potential¹⁶⁷.

[H3] Rationalizing free energy diagrams

When reading free energy diagrams, a distinction should be made between electrochemical steps and non-electrochemical steps. The thermodynamic barrier ΔG_{step} , which is the most uphill step in free energy along the reaction pathway, can be set as a lower bound for the true activation energy, ΔG^\ddagger . As mentioned, a free energy diagram for electrochemical N₂ fixation with a thermodynamic barrier greater than $\Delta G_{step} = 1.5$ eV under ambient conditions should be treated with skepticism.

Moreover, it is also important to consider the adsorption free energy of the inert N₂ molecule, an essential first step of N₂ fixation. N₂ physisorbing to the surface corresponds to an energy penalty of 0.67 eV¹⁶⁸ at 25 °C owing to the gas-phase entropy loss, and thus must be compensated by an enthalpic gain. To assess the point where N₂ adsorption becomes rate-limiting, we resort to collision theory to obtain the rate of collisions between a gas and a surface⁶³. Thus, the number of successful collisions per unit time per area becomes:

$$r \sim \frac{P_{N_2}}{N_A \sqrt{2\pi m k_B T}} \exp\left(-\frac{\Delta G_{*N_2}}{k_B T}\right) [\text{mol}_{N_2} \text{ cm}_{\text{geo}}^{-2} \text{ s}^{-1}]$$

where P_{N_2} is the partial pressure of N₂, m is the mass of N₂, k_B is the Boltzmann constant, T is the temperature, N_A is the Avogadro constant, and ΔG_{*N_2} is the thermodynamic N₂ adsorption free energy, which is a lower bound for the true adsorption barrier. To obtain the number of successful collisions per site per second, the rate can be multiplied by the Avogadro constant (N_A) and divided by the site density N_0 . Using a typical site density⁶³ of $N_0 = 1.5 \times 10^{15}$ sites/cm_{geo}² and 1 bar of N₂, the barrier corresponding to 1 successful collision per site per second (i.e. turnover frequency of 1 s⁻¹) becomes roughly 0.5 eV at 25 °C. In the case of aqueous solutions, the collision rate can be estimated by using the concentration of dissolved N₂ at standard conditions ($P_{N_2} = 0.012$ bar), leading to the requirement that the N₂ adsorption free energy should be below 0.35 eV to ensure that N₂ adsorption is not rate limiting.

[H1] Applications

Electrochemical, photo(electro)chemical and thermochemical N₂ fixations have primarily been discussed in this Primer due to the size of interest and research efforts in these fields, and the possibilities they offer to sustainably produce high value N-containing chemicals. Particularly power-to-NH₃ is an attractive process, as NH₃ is not only a fertilizer, but can also be used to power an NH₃-based economy, since it forms a liquid under light pressure and cooling, thereby providing a carbon-free and energy-rich fuel. This fuel can be transported and stored much easier and safer than liquid H₂, the only other viable carbon-free green fuel, and comparatively, NH₃ even contains a higher volumetric energy density. It can therefore provide power-plants a sustainable fuel for the generation of electricity, it can be used as fuel in gas turbines and power generators, or the NH₃ can be split, thereby providing a source of H₂ gas for fuel-cell based vehicles and marine transportation^{169,170}. Centralized production of NH₃ via the Haber-Bosch process is currently slowly replacing the H₂ supplied via steam-reformed methane (called brown NH₃) to water electrolysis driven by solar- and wind-powered electricity (Gen 2, Figure 1)²⁸. These electrified Haber-Bosch facilities would significantly reduce the carbon footprint of NH₃ production²⁹, and with the addition of e.g. NH₃ pipelines, the ease of storage and distribution could lead to the envisioned NH₃ economy. Thermochemical N₂ reduction is a crucial key point, as lowering the required pressure and temperatures of the Haber-Bosch process enables smaller and thereby cheaper production facilities¹¹. For fully decentralized NH₃ production of e.g. 1 device per farm or greenhouse for fertilizer production, significant breakthrough in electrochemical or photo(electro)chemical N₂ activation (Gen 3, Figure 1) is necessary¹⁷¹. These processes would completely eliminate the dependence on Haber-Bosch on a local scale, as the only inputs should be air, water, and renewable electricity on a small-scale device. Breakthroughs on this scale would also lead to electricity storage as NH₃, aiding the intermittency issue of renewable electricity sources, and more advances in overall power-to-X technologies, as more infrastructure and reliance on blue NH₃ will increase understanding of general electricity conversion, energy storage, and reconversion pathways. Overall, progress in the N₂ activation reactions has the capability of shaping a future without dependence on fossil fuels, as NH₃ is one of the leading choices for a carbon-free fuel.

[H1] Reproducibility and data deposition

[H2] The importance of reproducibility

Ensuring complete account and mitigation of contamination sources is key to improving reproducibility in N₂ activation. Given the ubiquity of N-impurities, results of catalytic performance must be accompanied with experimental details showing how contamination sources have been mitigated. Reporting the actual product concentrations and the measured concentrations in control experiments is also recommended, along with the electrolyte volume and the mass and surface area of the catalyst used, as these can be a telling factor toward contamination. More vitally, we emphasize the need to perform complete isotope-labelling experiments, with time-dependent product quantification and proper cleaning of the ¹⁵N₂ gas steams, to ensure unambiguous certainty of successful N₂ fixation. Additionally, more rigor needs to be applied in performing electrochemical and photo(electro)chemical measurements and their product detection measurements, especially when the reported selectivity is close to zero. For electrochemical measurements, the pre- and post-test Ohmic resistance can differ substantially due to bubble formation, temperature variance, etc., and thus the shift in potential should be properly adjusted⁷⁶. Similarly, in thermochemical studies, catalyst preparation-pretreatment and activity measurements are two main factors influencing the reproducibility of the experiments. Experimental details associated with these must be reported.

It is vital that one demonstrates $n \geq 3$ reproductions of the reported data, which include at least three repeated measurements in product detection for each catalytic activity point, three independent activity testing, and three independently prepared catalyst batches. The mean and spread of each data point must be reported, acknowledging errors from activity measurements and product detection, with the appropriate number of significant figures. This is significant as several studies report an excessive number of digits beyond the accuracy usually attainable in catalysis.

[H2] Data deposition and reporting

Transparency in reporting and data deposition are essential. Useful figures of merit regarding the catalytic performance and details of the experimental conditions, as elaborated in Table 2, must be reported to enable thorough assessment of the experimental rigor and aid comparisons of data collected under different conditions. Extra care must be given for electrochemical, photochemical, photoelectrochemical, and low-temperature thermochemical systems by clearly reporting the gas purity, the cleaning procedure of the gas (especially $^{15}\text{N}_2$ used in isotope-labelling experiment), and the actual concentration of the measured product. Ultimately, these efforts are aimed at evaluating the $mass_{prod}$ relative to the $mass_{sys}$ of the experiments. Kinetic measurements such as the determination of reaction orders and activation energy may be required according to the need of research. Lastly, pre- and post-measurement (and/or in situ) characterization of the catalyst may be necessary, to ascertain changes associated with the reaction conditions.

In a move towards open data, we also request the sharing of raw calibration and test data associated with catalytic activity measurements, the relevant data analysis scripts where possible, and results such as converged atomic coordinates and vibrational frequencies when a DFT calculation is performed.

[H1] Limitations and Optimizations

[H2] Cost of isotope experiments

For repeated isotope labelled experiments, the cost of $^{15}\text{N}_2$ can unfortunately be prohibitively expensive, as a single long-term experiment can easily cost upwards to 2,300 USD for 5 L. This can be circumvented by introducing a glass circulation pump. Once a high enough $^{15}\text{N}_2$ atmosphere is achieved in the system, the glass pump will continuously circulate the gas, without the need to supply more throughout the experiment. Furthermore, the circulation pump has the added benefit of not introducing contaminants over time, if the gas stream contains any NH_3 or NO_x species, decreasing the possibility of false positives. The glass circulation pump can be made in-house¹⁷² as seen in Figure 10a, or bought commercially.

Isotopically labelled $^{15}\text{N}_2$ can contain significant amounts of both $^{15}\text{NH}_3$, and $^{15}\text{NO}_x$ species that reduce easily, leading to isotopically labelled contamination⁹⁶. We do not advocate the use of aqueous solutions to clean N_2 , as they would not trap all contaminants¹⁷³. The residence time of the bubbles compared to the diffusion time inside the bubbles would need to be ideal, with certain probability of uptake. The bubbles need to be tiny, so they rise slowly and have fast internal mixing and large surface/volume ratio¹⁰¹. Furthermore, it is unclear how NO_x species would be trapped in acid¹³³. We found that a home-made reduced Cu catalyst combined with a freeze trap to be efficacious for removing impurities, on the basis of the measured level of all NH_3 and NO_x impurities removed before and after the cleaning⁷⁶. The reduced Cu catalyst will catch all NO_x species, while the cold trap freezes out NH_3 . Commercial gas purifiers down to ppt per volume fraction (pptV) level are also available for purchase. A complete home-built and inexpensive system for both the glass circulation pump and the reduced Cu catalyst is shown in Figure 10b.

[H2] Access to NMR

NMR is the most commonly reported technique for isotope labelling experiments, as it can distinguish between $^{14}\text{NH}_3$ and $^{15}\text{NH}_3$. Not all will have access to a high-field 800 MHz NMR, but the use of the more commonly available 400 MHz NMR can achieve similar sensitivity, covered in more detail in Reference⁷⁶.

[H1] Outlook

[H2] Adoption of standardized test protocols for N_2 activation

N_2 reduction and oxidation at low temperature and pressure are reactions with immense technological significance. Unfortunately, much published research lacks rigorous and standardized testing, leading to possible contamination of results and false positives. The possibility of contamination is particularly prominent for reports with low product formation rates, spanning all electrochemical and photo(electro)chemical systems to date, as well as some low temperature thermochemical systems. The only conclusive proof of successful N_2 activation is via repeated and quantified isotope labelled testing with proper gas cleaning. In this Primer, our objective is to define the cut-off necessitating the use of the crucial $^{15}\text{N}_2$ quantitative isotope labelling experimentation for all N_2 activation reactions. The cut-off is defined at $mass_{prod} > 2 mass_{sys}$, where $mass_{sys}$ is based on experimentally measured N in the system. Furthermore, the concentration of the product must also exceed 100 ppm, far above the olfactory detection of NH_3 , to circumvent contamination from other sources. This will prevent false positives from reaching publication, as these results hinder development of the N_2 activation field.

Beyond electrochemical, photo(electro)chemical and thermochemical systems, efforts on non-thermal plasma N_2 fixation have been pursued in recent years¹⁷⁴. Generally, the plasma-driven N_2 fixation studies report product concentrations of hundreds of ppm and up to ~5% of the gas stream³⁷, diminishing the detrimental contribution of labile N-species in various contamination sources. However, with the field's primary focus on racing toward higher energy efficiency, several studies using dielectric barrier discharges as the most common plasma source show worryingly low NH_3 production ($C_{prod} < 100$ ppm)³⁶, possibly dipping into the range of contaminants. Moreover, the mechanochemical method of NH_3 synthesis has emerged as a new direction for N_2 activation^{40,41}. The reported NH_3 yields are similarly high, but the field can benefit from the critical assessment of the potential size of N-contaminants. We suggest researchers also adapt the protocol in this Primer by comparing the product mass ($mass_{prod}$) with the total equivalent N mass of the system ($mass_{sys}$) and performing quantitative isotopic-labelling verification technique at the low-yield data points to warrant genuine N_2 fixation.

[H2] Mechanistic insight via in-situ measurements

Our insight into the reaction mechanisms on N_2 reduction has largely been built on theoretical investigations^{69,73,175}. In-situ and in-operando techniques to probe intermediate species can validate or challenge established paradigm, and inform valuable insights into future catalyst designs (Box 2). However, adoption of the rigorous protocol takes precedence to ensure what is being detected is not associated with the presence and redox processes of adventitious N sources.

[H2] Perspective to achieve commercialization

The emerging false positives and likely unreliability of many prior publications in the field of N_2 fixation have undoubtedly injured the reputation of the field. In the immediate future, the scientific community should aim to restore the field's integrity and eliminate the emergence and propagation of unreliable results. In our view, this can be achieved through increased rigor of experimental practices, increased efforts to reproduce reported results, increased cross-pollination of knowledge and best practices across laboratories, and a more deliberate regard toward fundamental concepts and principles.

In the next 5-10 years, we anticipate researchers will focus on addressing the field-specific needs (Box 3), and ultimately finding breakthrough catalysts with practically relevant and reliably demonstrated yield rates, selectivity, stability and energy efficiency to enable industrial deployment of sustainably-produced ammonia. The obsessive pursuit of breakthrough results must go hand in hand with robust fundamental studies unveiling the identification of true reaction mechanisms and active sites and reaction kinetics, aided by experimental mechanistic studies and quantum chemistry or other computational methods. Ultimately, concerted efforts from experimental and theoretical communities will be key to discovering a practical solution to decarbonize the fixation of N₂.

Boxes

[bH1] Box 1. Sources of system N mass

$mass_{N,cat}$	The amount of measured N in the catalyst and support, which must be experimentally determined. This measure is important, even if the catalyst does not intrinsically contain N, as substantial levels of NO_3^- and nitrides can contaminate commercial metal sources ^{106,176,177} , despite manufacturer's claims otherwise. We recommend the simple 2 step procedure by Chen <i>et al.</i> ¹⁷⁷ of alkaline and acidic treatment of the catalyst, followed by HPLC or UV-vis analysis, or any equivalent method for determining N-content. Special care should be taken regarding N-buildup on the catalyst if pretreated with an N-containing procedural step. These N-species could contaminate the catalyst, and convert to NH_3 in a non-catalytic way ^{178,90} . We therefore recommend examining the N-content of the catalyst as bought, after any pre-treatment, and after catalysis. If the N-content of the catalyst is not explicitly experimentally determined, one should consider $mass_{N,cat}$ as at least 25% of the whole mass of the catalyst, unless the catalyst is intrinsically N-containing (e.g. a nitride), in which case 100% of the mass should be considered.
$mass_{N,electrolyte}$	The measured amount of N in the electrolyte. Electrochemical and photo(electro)chemical systems submerge the catalyst in electrolyte, and if the electrolyte itself contains N species, these must be considered as sources of contamination, due to possible electrolyte breakdown. However, the electrolyte itself may also be contaminated, as chemicals and membranes (e.g. Nafion) readily soak up NH_3 from the surroundings ⁷⁶ , and both NO_x and NH_3 blank measurements of the electrolyte should be included with each batch of electrolyte.
$mass_{N,absorber}$	The measured amount of N in the photoabsorber present in photo(electro)chemical system. This may contain sources of activated N as a contaminant, and should be determined experimentally.
$mass_{N,gas}$	The total calculated N impurities of the N_2 gas stream ^{96,101} . If the purity of the N_2 is e.g. 99.999%, one must consider 0.001% of the total gas used to be 100% contamination, and calculate the mass of this based on flow rate and duration. Alternatively, a proper gas cleaning procedure, with reported NH_3 and NO_x contamination of the gas before and after cleaning can be used.

[bH1] Box 2. In-situ and operando techniques for N_2 fixation

Surface enhanced infrared spectroscopy (SEIRAS)	SEIRAS can detect many of the adsorbates in electrochemical N_2 fixation in operando. The IR adsorption peaks can be attributed to vibrational modes of reaction intermediates, and these signals can be enhanced on metal surfaces by the SEIRAS effect ¹⁷⁹ . Several studies have attempted SEIRAS for electrochemical N_2 reduction ^{180,181} , but contributions from contamination to the detected species are highly probable. Nonetheless, Matsui <i>et al.</i> have demonstrated successful <i>in-situ</i> FTIR spectroscopy for electrochemical NH_3 oxidation on Pt electrode ¹⁸² . Here, various bands, detected at different voltages, were ascribable to the HNH bending mode of *NH_3 , NH_2 wagging mode of *N_2H_4 , absorption of NO bridged species and HOH bending mode of *OH groups.
Electron Paramagnetic	EPR allows the monitoring on paramagnetic species as a function of potential in an electrochemical process, detectable upon rapid freezing of the electrodes. EPR spectra have detected nitrous oxides in redox processes in biomolecules ¹⁸³ and

Resonance Spectroscopy (EPR)	during alcohol oxidation. ¹⁸⁴ Electrochemical EPR could potentially detect absorbed paramagnetic *NO species formed during N ₂ oxidation.
N₂ isotopic exchange reaction (N₂-IER)	N ₂ -IER (¹⁵ N ₂ + ¹⁴ N ₂ → 2 ¹⁵ N ¹⁴ N) has been used to probe the reaction mechanisms and the rate-determining step of the thermochemical NH ₃ synthesis, by introducing ¹⁴ N ₂ / ¹⁵ N ₂ gas mixtures and monitoring the ¹⁴ N ₂ , ¹⁵ N ₂ and ¹⁴ N ¹⁵ N gas phase composition. Successful examples of N ₂ -IER for NH ₃ synthesis have been reported on Fe ¹⁸⁵ and Ru ^{186,187} confirming N ₂ dissociation as the rate-determining step. A N ₂ -IER study on cobalt molybdenum nitride ¹⁸⁸ demonstrates the possible participation of lattice N in a Mars-van Krevelen mechanism.
Steady State Isotopic Transient Kinetic Analysis (SSITKA)	SSITKA is performed under steady-state conditions and involves introducing a step change in the isotopic content of the reactant and monitoring the transient responses of the isotopically labeled species ¹⁸⁹ SSITKA has been used to study the kinetics of NH ₃ synthesis on commercial Fe ¹⁹⁰ and Ru ¹⁹¹⁻¹⁹⁴ catalysts. A study on commercial Fe catalysts reveals *N as the most abundant reactive intermediate ¹⁹⁰ . The role of potassium promoter over Ru catalysts, investigated by SSITKA, is revealed to induce surface site heterogeneity on Ru/SiO ₂ , creating super-active sites responsible for enhanced catalytic activity ¹⁹¹ .

[bH1] Box 3. Field-specific progress, needs, and insight

Thermochemical N ₂ reduction	The thermochemical N ₂ reduction reaction is the most advanced in terms of technological readiness, as there are a variety of newly developed catalysts shown to produce NH ₃ at low pressures (1-10 bar) and low temperatures (< 300 °C). However, this type of reaction would still require higher operation temperatures (compared to ambient conditions) and pure H ₂ as the feed gas, necessitating an additional clean H ₂ production step. Increased focus is on exploring unconventional, highly active, and electron-rich materials as catalysts or catalyst supports in the aim of optimizing the reaction rate, decreasing the temperature even further. In the meantime, efforts should be devoted to the elucidation of active site and reaction mechanism. As a bellwether reaction, any progresses in fundamental insight and/or practical transformation in thermochemical NH ₃ synthesis would have profound impact on the field of heterogeneous catalysis.
Electrochemical and photo(electro)chemical N ₂ reduction	Reactions that use protons in lieu of H ₂ have also been gaining increased attention. The requirements for high yields comparable to the Haber-Bosch process or even to thermochemical systems is not necessary, as the focus is on creating completely decentralized systems ²⁸ . Unfortunately, there is a strong need to validate the aqueous results using rigorous protocols ^{76,101} , in light of the sheer selectivity challenge against H ₂ evolution in aqueous environments as revealed by theory and the ubiquity of N-containing contaminants. Once these systems are experimentally validated, efforts towards increased catalytic activity, selectivity, and number of active sites can be considered ¹²⁴ . The non-aqueous Li-mediated N ₂ reduction process have been proven to work, achieving the highest reported energy efficiencies in the literature. However, this system has significant kinetic challenges due to sluggish mass-transport limitations, which needs to be overcome for practical commercial use.
Electrochemical N ₂ oxidation	Electrochemical aqueous N ₂ oxidation is piquing the curiosity of the scientific community. Nonetheless, we consider this field to still be in its infancy, with ample opportunity for fundamental insight and step improvements to catalyst performance.

Tables

Table 1 Common sources of contamination of electrochemical and photo(electro)chemical systems and the suggested method of elimination. Methods adapted from Liu *et al.*¹⁰⁶

Sources of Contamination	Nitrogen form	Method of Elimination
Feed gas ⁹⁶	NO _x , N ₂ O and NH ₃	Use of home-made reduced Cu catalyst and a freeze trap, or commercial gas purifier
Impurities in the catalyst ^{90,176,177}	NO _x ⁻ and NH ₄ ⁺	Complete removal via pre-reduction of the catalyst before NRR testing
Uptake/release from the membrane ^{76,105,106}	NH ₃	Replace with contamination-free membrane (such as Celgard)
Electrolyte	NH ₄ ⁺ , NO ₂ ⁻ and NO ₃ ⁻	Removal via annealing of electrolyte salt or other cleaning methods
Glassware, tubes, laboratory air, etc. ¹⁹⁵	NH ₃	Ensure the entire system is properly cleaned between uses, e.g. by boiling in ultra-pure water and drying in oven

Table 2. Required reporting standards across the different catalyst system types used for nitrogen reduction and oxidation.

Data type	Definition	System type
Reporting of catalyst performance		
Yield rate	Amount of product formed in a given time interval	All systems
Area-normalized activity	Yield rate normalized to either geometric or electrochemically active surface area	Electrochemical
Mass-normalized activity	Yield rate normalized by the mass of catalyst	All systems
Turnover frequency	Rate of chemical conversion normalized to number of actives per unit of time.	All systems
Faradaic efficiency	Ratio of charges employed for the synthesis of a given product relative to the total amount of charge passed through the circuit.	(Photo)electrochemical
Stability	Capability of a catalyst to perform in prolonged time intervals without detriment in its intrinsic activity	All systems
Energy efficiency	Ratio of converted energy relative to the initial energy input.	All systems
Average Quantum yield	Ratio of electrons transferred towards product relative to the incident photons reaching the sample at a given wavelength	Photo(electro)chemical
Incident photon-to-current efficiency	Ratio of produced photocurrent versus the incident photon flux at a given wavelength.	Photo(electro)chemical
Reaction orders	The power dependence of the reaction rate on the concentration of each reactant.	All systems
Activation energy	The minimum amount of energy required to activate atoms or molecules to a state in which they can undergo a chemical reaction.	All systems
Reporting of experimental conditions		

Catalyst loading	Mass of catalyst employed in a single experiment	All systems
Gas Purity	Purity of the $^{14/15}\text{N}_2$, H_2 and Ar gases used in the experiments.	All systems
Time	Length of time of the experiment	All systems
Potential	The operating potential of working electrode during reaction	Electrochemical
Electrolyte volume	The volume of electrolyte used in the catalytic measurements	(Photo)electrochemical
Temperature and pressure	The temperature of the catalyst bed and the total pressure of the reaction gases.	All systems
Photon intensity	Photon flux reaching the sample per second and illumination area	Photo(electro)chemical
Illumination area/distribution	Available surface for the incident photon flux to reach the sample	Photo(electro)chemical
Weight hourly space velocity	Flow rate of the reaction gas fed to the reactor, divided by the mass of catalyst	Thermochemical (most relevant)
Other Information		
Gas cleaning procedure	A detailed account of how impurities are removed in the gas streams	All systems
Catalyst characterization	Structural or chemical information pre- and post- catalytic measurement to inform changes to the catalyst	All systems

Figures

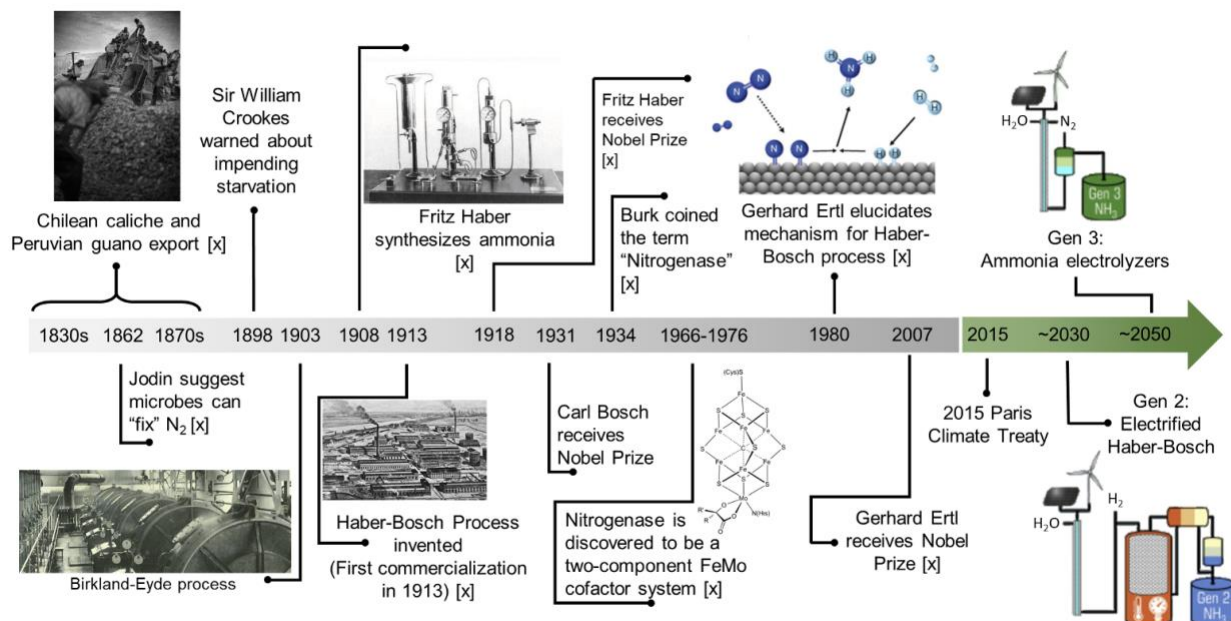
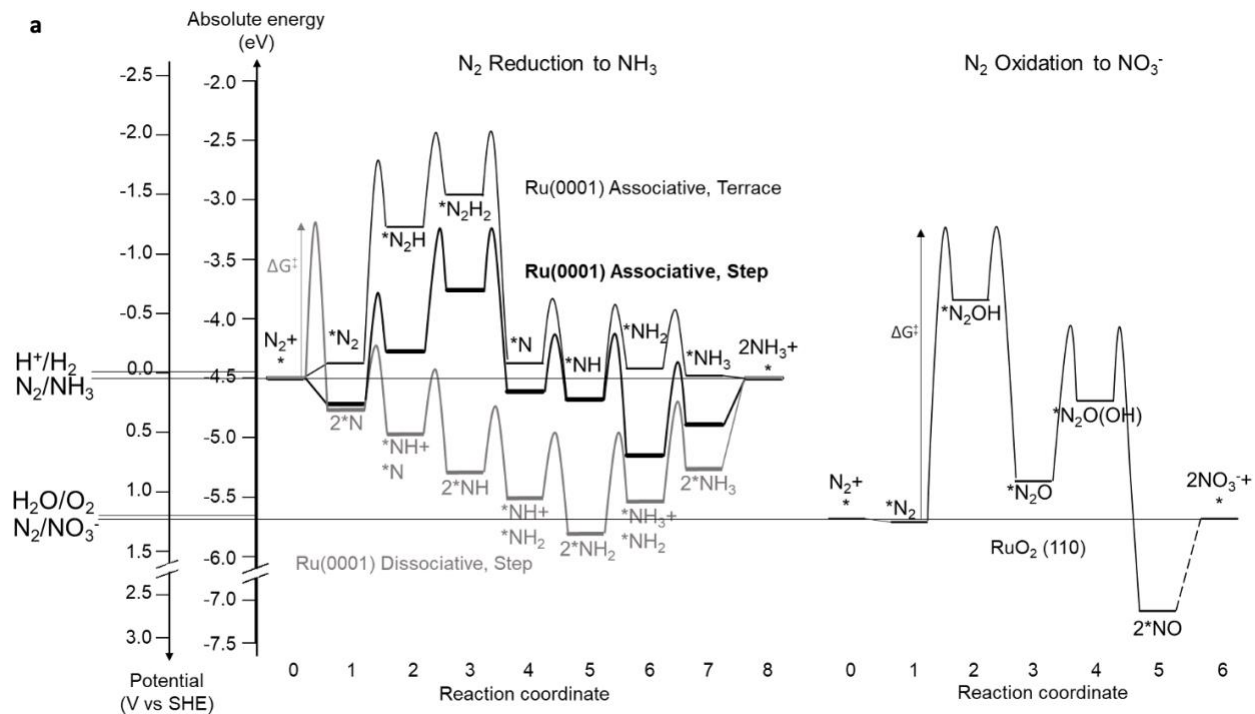


Figure 1. Historical development of N_2 activation. Nature mainly produces activated N-species via the nitrogenase enzyme⁶. The source of N-containing fertilizer first originated from caliche deposits and guano, both predicted to be unsustainable⁸. Two commercial N_2 reduction processes emerged in early 20th century: the Birkland-Eyde and Haber-Bosch process, and the latter has since dominated the N_2

activation industry⁷, with 3 Nobel prizes given for its discovery¹⁴. With the global commitment to tackle climate change, the decarbonization of nitrogen fixation is envisioned to involve two technology generations: Coupling of Haber-Bosch with renewable H₂ (Gen 2) and electrochemical NH₃ synthesis (Gen 3)²⁸.



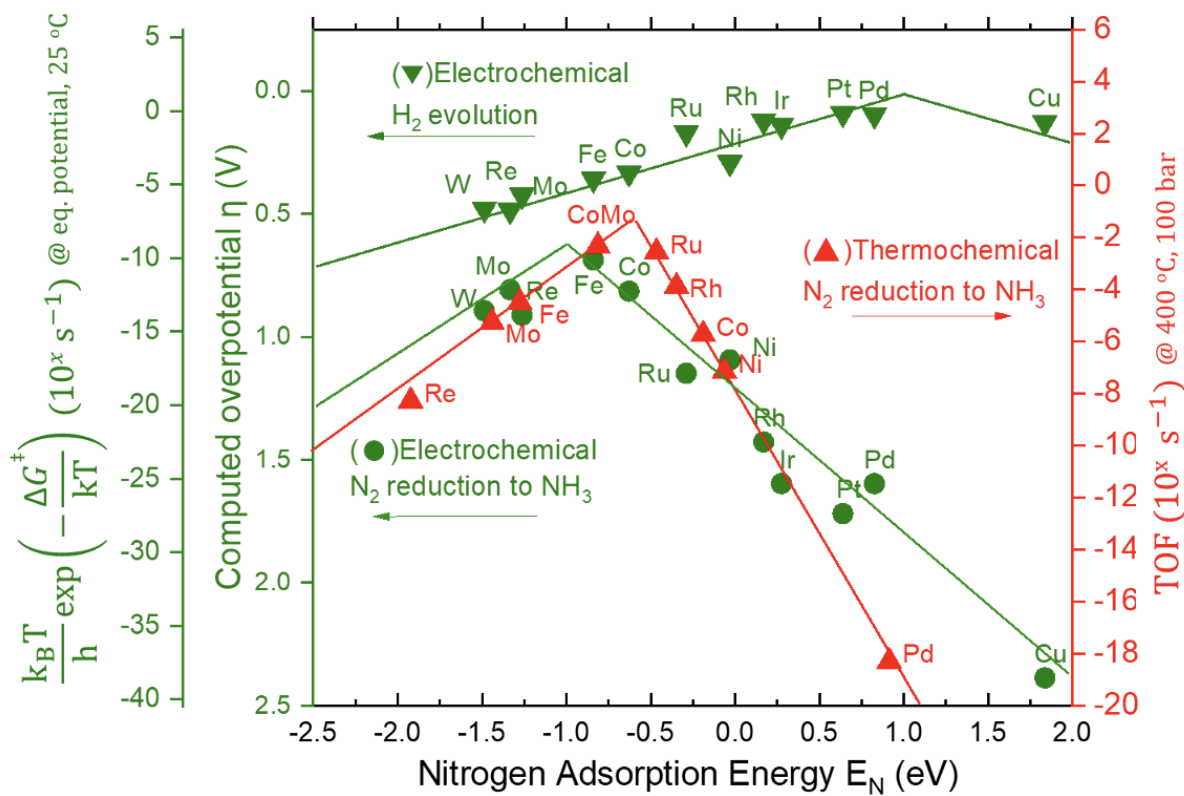
b

Figure 2. The fundamental challenges of N₂ activation **a)** Standard equilibrium potentials for N₂ and H₂O redox are aligned with the electron energy (0 V_{SHE} equals -4.44 eV on the absolute scale where electron in vacuum is 0 eV⁴³). The free energy diagrams for N₂ reduction⁷⁴ and oxidation⁵⁶ on selected surfaces are plotted at the equilibrium potential referenced to standard conditions, 1 bar NH_{3(g)} and 1M H⁺NO_{3(aq)}. *X refers to surface adsorbed intermediates. The energy difference between two states (e.g. step 1-2 of associative N₂ reduction) corresponds to the thermodynamic barrier and can be lowered by potential if the step involves an electron transfer. An additional activation barrier may be present, shown as bumps between steps, whereby the value 0.7 eV is chosen for all coupled proton-electron transfer steps (consistent with Singh et al⁶⁶). The N-N dissociation barrier is chosen as per ref¹⁹⁶. The overall reaction barrier can be approximated by the step with the highest barrier (ΔG^\ddagger), which is much slower than other elementary steps thus governing the rate. **b)** Limiting potential analysis⁶⁶ for electrochemical N₂ reduction (overpotential referenced to N_{2(g)}/NH_{3(g)}) and H₂ evolution (overpotential referenced to H^{+(aq)}/H_{2(g)}) as a function of N binding energy on transition metal terraces. For electrochemical N₂ reduction, N₂+*+H⁺+e⁻ → *NNH (Step 1-2 in a) and *NH+H⁺+e⁻ → *NH₂ (Step 5-6) define the right and left legs respectively. For H₂ evolution, *+H⁺+e⁻ → *H and *H+H⁺+e⁻ → H₂ define the right and left legs respectively. The rate constants are shown in the second green axis, where kT/h equals 10¹³ at 25 °C. The red points correspond to the calculated turnover frequencies (TOF) on transition metal FCC/HCP (211), computed using a micro-kinetic model by considering the dissociative mechanism as described in ref⁶⁹. The synthesis condition is 400 °C, 100 bar, gas composition H₂:N₂=3:1 containing 5% NH₃.

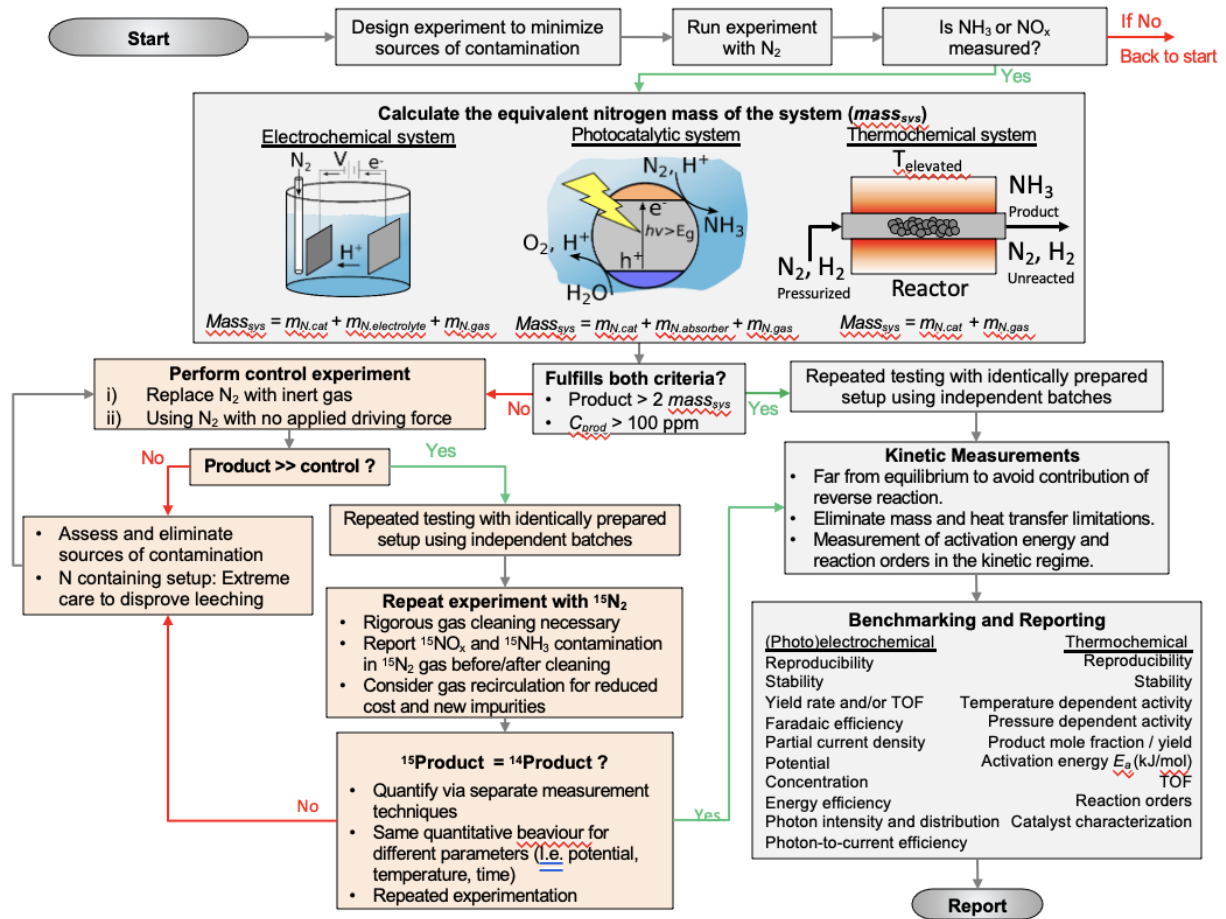


Figure 3. General flow chart of experimentation. The total equivalent mass of the system, $mass_{sys}$, must be determined, which will be compared with the amount of product (NH_3 or NO_x) measured, $mass_{prod}$, in order to determine the need for isotope labelled experiments. The $mass_{sys}$ is the summation of the relevant N-containing masses, which includes the experimentally measured N in the catalyst ($m_{N,cat}$), the mass of N in the electrolyte ($m_{N,electrolyte}$), the mass of the N-containing absorber ($m_{N,absorber}$), and the calculated or measured mass of impurities in the gas stream ($m_{N,gas}$).

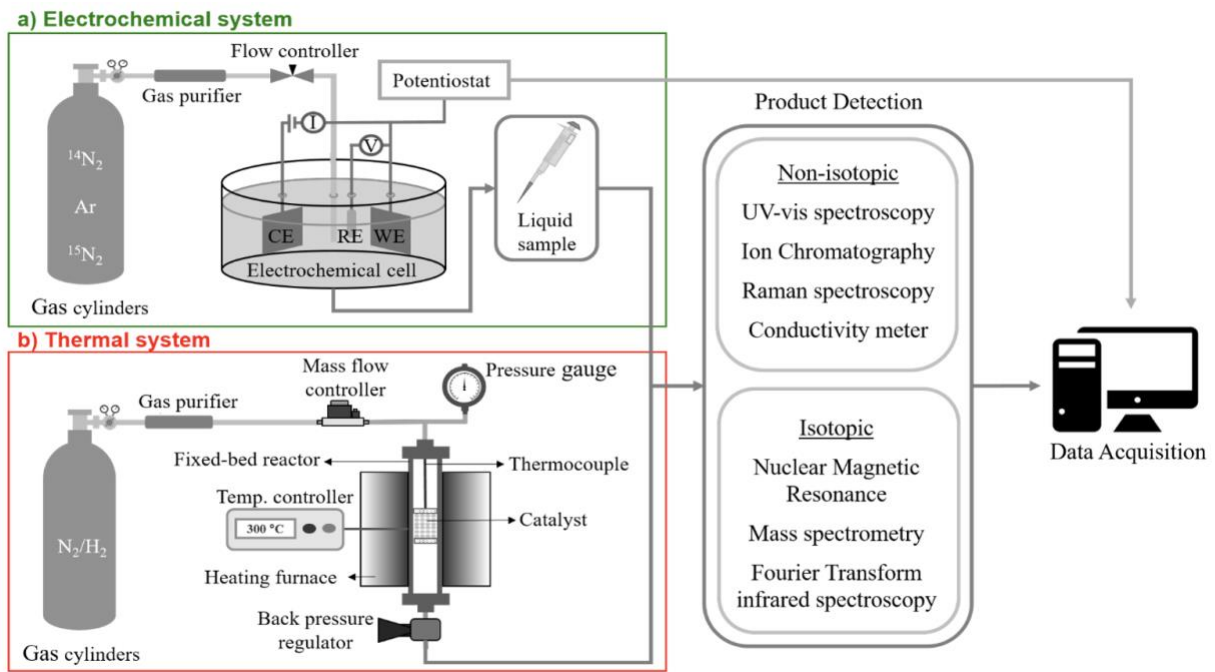


Figure 4. Experimental setup for electrochemical and thermochemical N_2 activation. a) Experimental setup for electrochemical N_2 reduction or oxidation reactions. The gas passes through a gas cleaner (either a reduced metal catalyst and freeze trap, or a commercial purifier), then flows into the electrochemical cell with a defined flow rate. The setup can be adapted for photoelectrochemical systems by using a photoelectrochemical cell with an illumination source. The reaction of interest is undertaken by controlling the potential across the electrodes via a potentiostat. For photochemical systems, the setup does not require a potentiostat, and the cell typically contains a suspension of particles or a surface with the active catalyst, and an illumination source is used to drive the reaction. b) Activity measurement system for thermal NH_3 synthesis. The setup contains a fixed-bed reactor, a furnace with a temperature controller, a thermocouple placed on the top of catalyst bed, gas purifiers, a flow meter, a pressure gauge and a back-pressure regulator. Then, for any catalytic system, the product of catalysis is detected via either non-isotope or isotope-sensitive techniques if necessary.

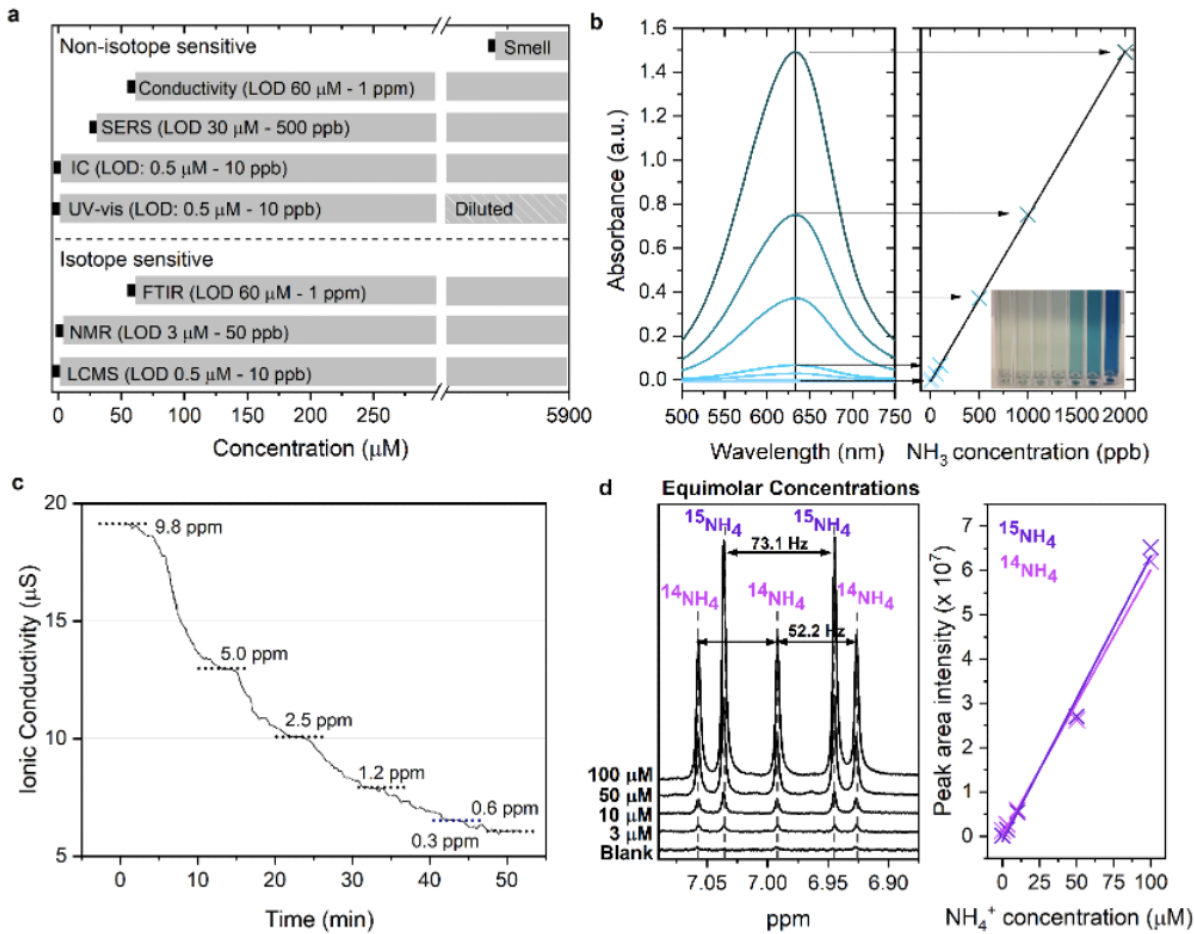


Figure 5. Isotopic and non-isotopic ammonia detection methods. a) Detection limits of well-known techniques for NH_3 quantification. The bar at 5882 μM (100 ppm) corresponds to NH_3 concentrations in liquid where olfactory detection is possible beyond any doubt⁹⁵. UV-vis⁷⁶, Conductivity meter¹¹⁹, and nuclear magnetic resonance (NMR)⁷⁶ is discussed in text, Fourier transform infrared spectroscopy (FTIR)⁸³, liquid chromatography mass spectroscopy (LCMS)¹⁹⁷, surface enhanced Raman spectroscopy (SERS)¹⁹⁸ and ion chromatography (IC)¹⁹⁹ is discussed in the SI. b) UV-vis spectra of indophenol blue method, showing quantification via calibrated samples from 10 to 2000 ppb NH_3 in H_2O . Straight line is fitted based on peak absorbance of each sample, displaying linearity with sample concentration. c) Conductivity measurement curve showing sensitivity of the NH_3 concentration from 9.8 to 0.3 ppm in purified H_2O ²⁰⁰. Due to the intensity of the conductivity baseline, it is difficult to detect an NH_3 concentration below 1 ppm. d) Example of NMR spectra of increasing equimolar $^{14}\text{NH}_3$ and $^{15}\text{NH}_3$ concentrations, clearly showing the respectively distinct triplet and doublet peaks. Calibration curve for $^{14}\text{NH}_3$ and $^{15}\text{NH}_3$ based on area under respectively the triplet and doublet peaks from the NMR spectra⁷⁶.

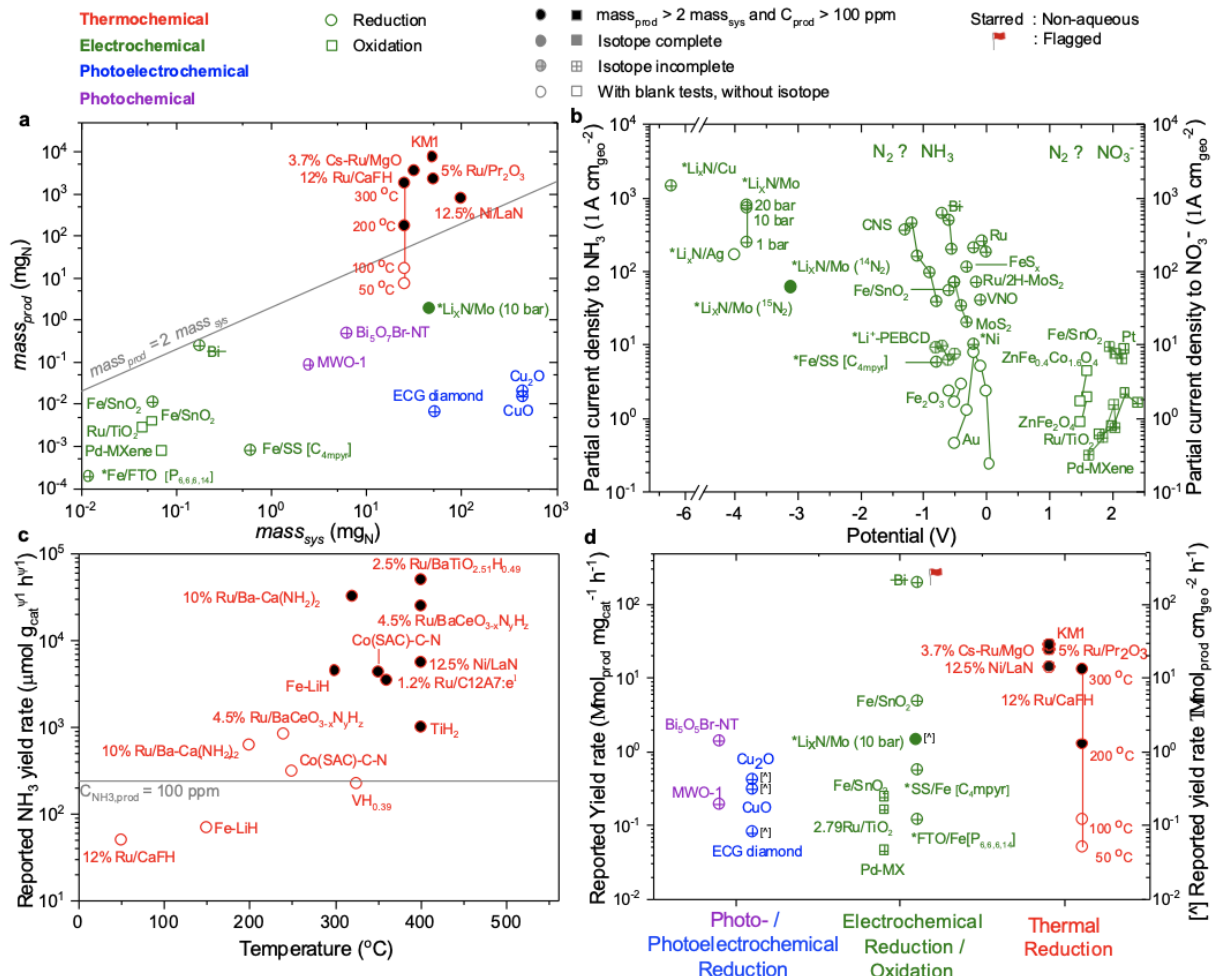


Figure 6. State-of-the-art literature overview of electrochemical, photoelectrochemical, photo(electro)chemical, and thermochemical N₂ activation Evaluation of experimental conditions for thermochemical (red), electrochemical (green), photochemical (purple), and photoelectrochemical (blue) N₂ fixation. Experimental details found in Table S1-3. Circle represents reduction, square represents oxidation. Unfilled symbol represents data with simple background tests. Cross represents data with either qualitative or quantitative isotope labelled experiments at a single point, without measuring or cleaning gas contaminants. Filled symbol represents repeated isotope labelled experiments with rigorous gas cleaning. Black-filled data satisfy both mass_{prod} > 2 mass_{sys} and product concentration above 100 ppm. Starred points contain non-aqueous electrolytes. Flagged data raise suspicion. **a)** Comparison of mass_{prod} with mass_{sys} for different catalytic systems. mass_{N,cat} calculated based on 25% catalyst weight for non-N-containing catalysts, and 100% for N-containing catalysts. Thermochemical data at 400 °C and 1 bar unless otherwise specified. **b)** Literature overview of partial current density towards NH₃ (left y-axis) or NO₃⁻ (right y-axis) from product detection as a function of potential vs RHE, unless otherwise specified. **c)** Literature overview of thermochemical NH₃ synthesis catalyzed by “reactive” materials whose composition or active phase may change during or after reaction. The line C_{NH3,prod} = 100 ppm was calculated with the assumption of WHSV = 60,000 ml g_{cat}⁻¹ h⁻¹. Data at 10 bar unless otherwise specified. **d)** Comparison of reported mass-specific activity. Yield rates of data points annotated by [] are expressed in μmol cm_{geo}⁻² h⁻¹. Fe on Stainless Steel (Fe/SS) and Fe/FTO¹³⁷ reported vs NHE, Li_xN/Cu⁸¹ total cell potential with Ohmic correction, Ni²⁰¹

vs Ag wire in 0.1 M LiCl/EDA, Li_xN/Ag^{138} is vs Ag/AgCl/AgCl (sat), LiCl, $LiClO_4/THF$ reference, $CsRu/MgO^{113}$ at 9 bar, $Ru/Pr_2O_3^{202}$ at 390 °C and 9 bar, $Ru/CaFH^{85}$ at 1 bar, $KM1^{148}$ at 10 bar, Mn_4N-LiH^{203} at 30 bar, TiH_2^{155} at 50 bar, 2.5% $Ru/BaTiO_{2.5}H_{0.49}^{154}$ at 50 bar, 4.5% $Ru/BaCeO_3-xN_yH_z^{204}$ at 9 bar, $Ru/Ba-Ca(NH_2)_2^{205}$ at 9 bar, 12.5% Ni/LaN^{153} at 1 bar, $VH_{0.39}^{156}$ at 50 bar.

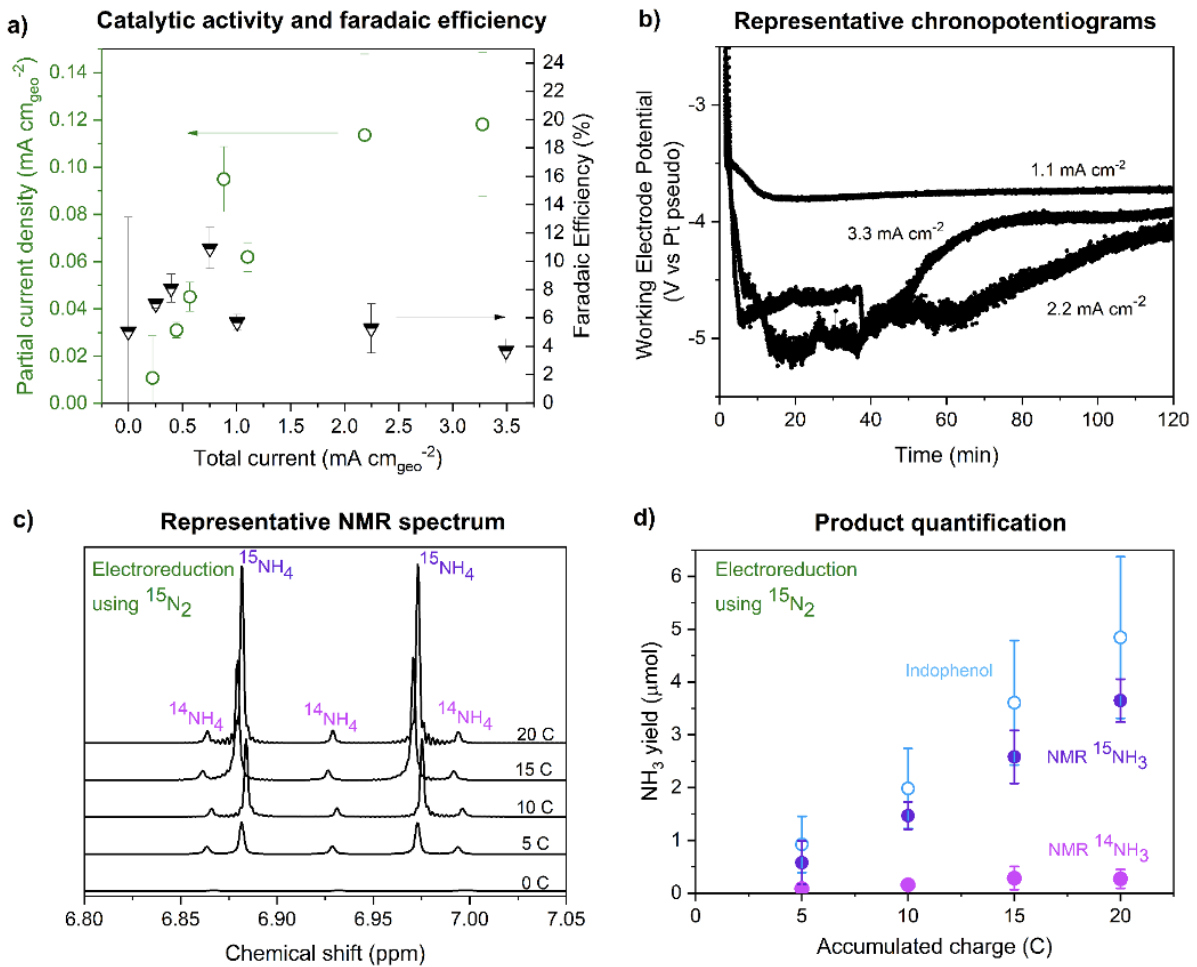


Figure 7. Example data of Li-mediated NH_3 synthesis in THF with $LiClO_4$ salt and EtOH as the proton source. a) Partial current density to NH_3 (i_{NH_3} , left y-axis) and Faradaic efficiency (FE_{NH_3} , right y-axis) as a function of total applied current. b) Representative CPs for experiments plotted in panel a). c) Representative NMR data from a single measurement, with samples taken every 5 C using cleaned $^{15}\text{N}_2$ as feed-gas. d) Yield of NH_3 as a function of charge passed, showing quantitative agreement between isotope sensitive results (purple and pink) with non-isotope sensitive result (blue). Error bars signify mean and standard deviation of 3 repeated identical but independently prepared experiments. a-b) replotted from Schwalbe et al.⁷⁹, c-d) replotted from Andersen et al.⁷⁶.

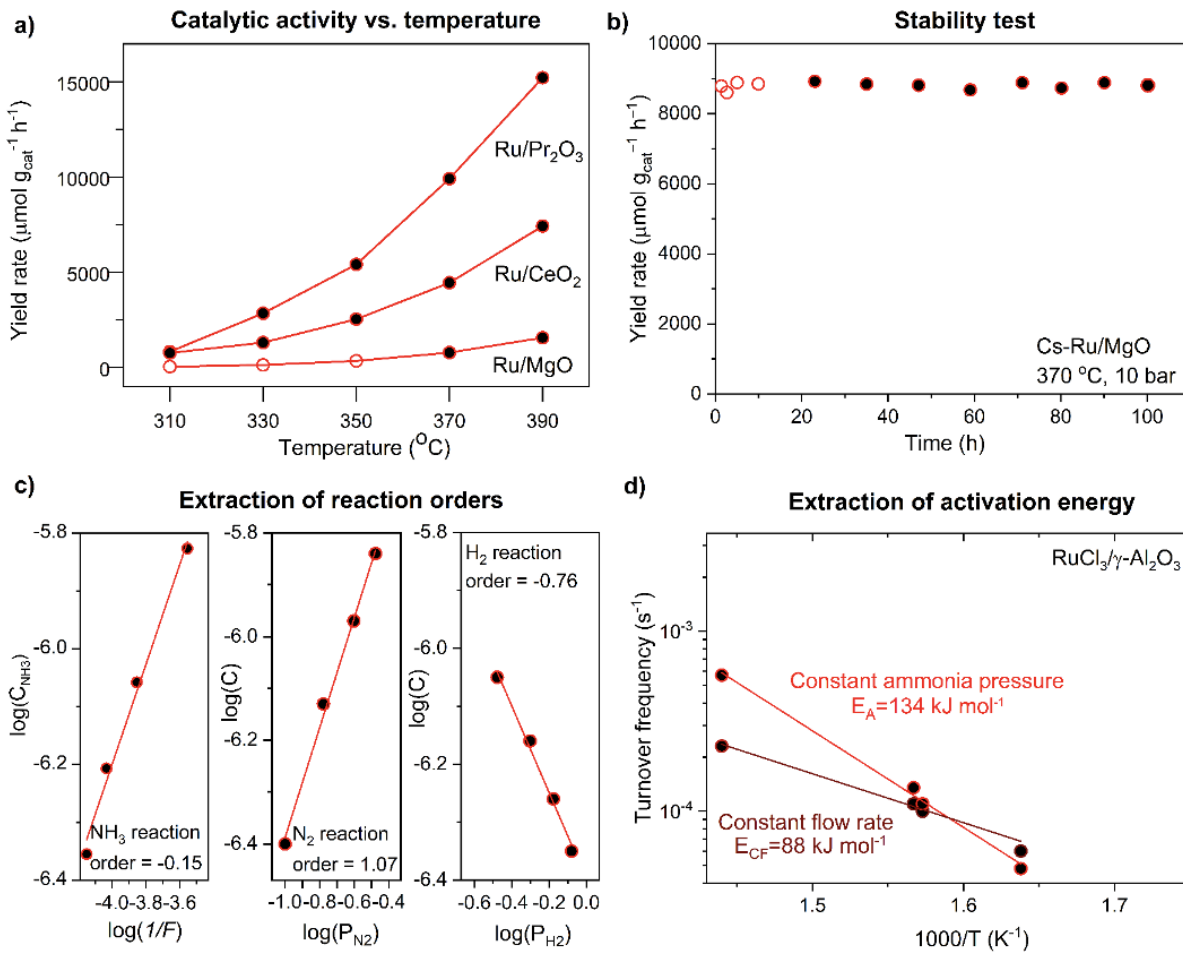


Figure 8. Recommended reports of catalytic performances for thermal NH₃ synthesis. (a) NH₃ synthesis rate as a function of temperature⁷⁸; (b) Stability test of NH₃ synthesis rate¹¹³ (c) extraction of reaction orders with respect to NH₃, N₂, and H₂²⁰⁶. Here, the term of $\log(r) - \alpha \log(P_{NH_3})$ is represented by $\log C$; (d). Arrhenius plots at constant NH₃ pressure (red) and at constant flow rate (brown) resulting in a difference in the extracted activation energy. Dark-filled points satisfy the $mass_{NH_3} > 2 mass_{sys}$ criteria.

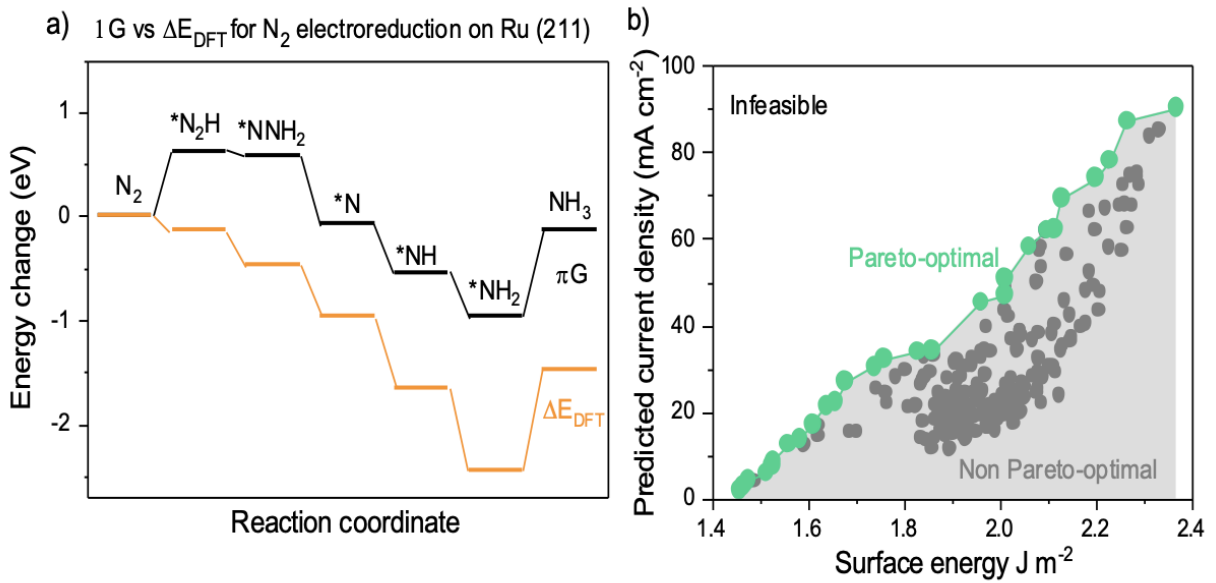


Figure 9. Density functional theory results (a) An energy diagram of N_2 reduction on Ru (211) showing the free energies and DFT energies respectively (black and orange respectively⁶⁵). (b) The surface energy plotted against the predicted current density for the O_2 reduction reaction on defected Pt (111) surfaces. Green points represent points on the Pareto Frontier, grey points represent non Pareto-optimal surfaces. The grey area represents sub optimal surfaces whereas the white region represents unobtainable surfaces¹⁶⁵. The current density (i) is calculated using the expression $i = i_c \exp(-\Delta G_{ORR}/kT)$, where i_c is an experimental value $3.68 \times 10^{11} \text{ kA mol}^{-1}$ at cell potential 0.9 V , and ΔG_{ORR} is the change in Gibbs energy of the limiting step. The surface energy of each defected surface is calculated by dividing the formation energy by the surface area. The full methodology can be found in Ref¹⁶⁵.

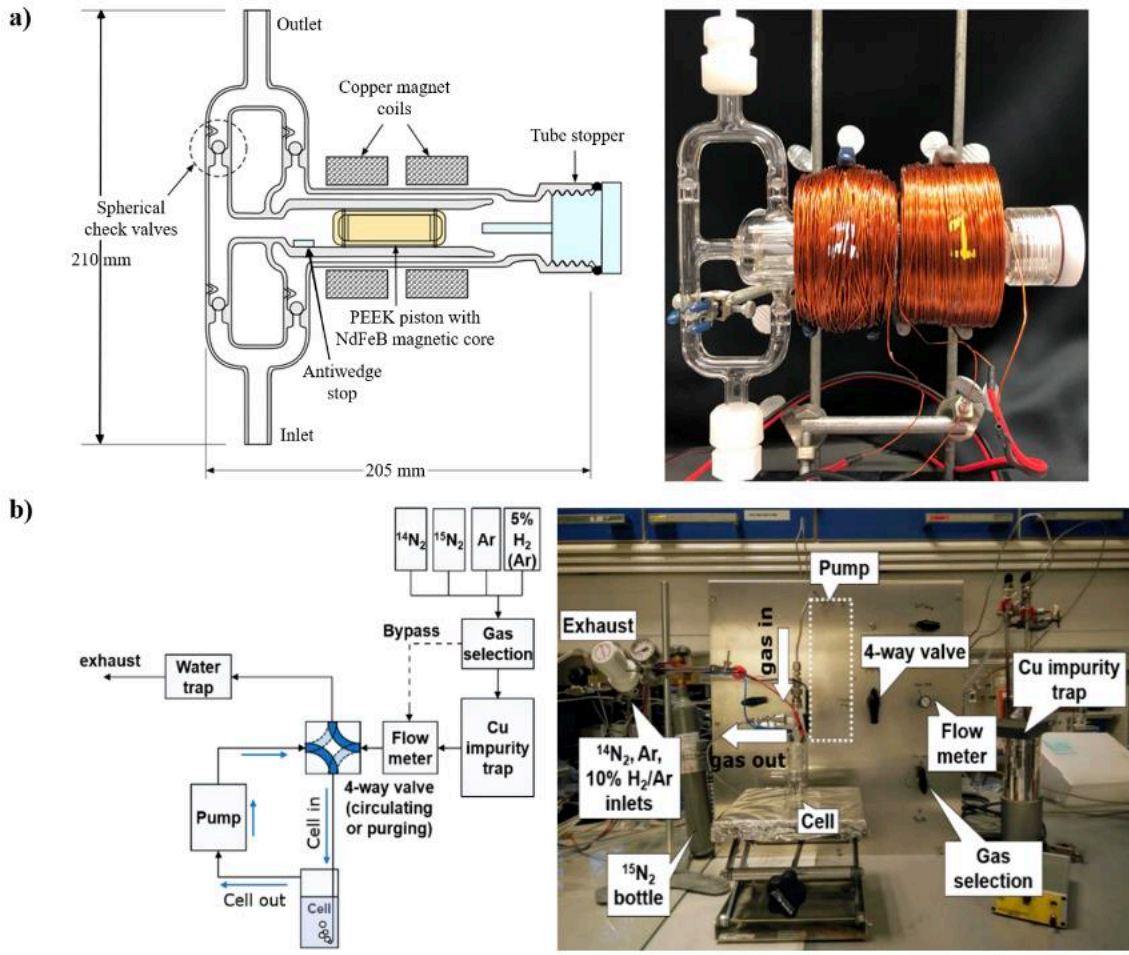


Figure 10. Home-built glass circulation pump and full gas recirculating setup with home-built activated Cu catalyst for gas cleaning. a) Glass circulation pump, enabling long-duration experiments without supplying continuous $^{15}\text{N}_2$. Republished with permission from Reference¹⁷². b) Inexpensive gas cleaning system with a reduced Cu catalyst, freeze trap and glass circulation pump for cheap $^{15}\text{N}_2$ experimentation. Reprinted with permission from Reference⁷⁶.

Acknowledgment

Y.S.- H acknowledges support by Toyota Research Institute through the Accelerated Materials Design and Discovery Program. H.I. acknowledges support from the Imperial–MIT Department of Materials Exchange Program. S.Z.A. and I.C. acknowledge funding by Villum Fonden, part of the Villum Center for the Science of Sustainable Fuels and Chemicals (V- SUSTAIN grant 9455) and Innovationsfonden (E-ammonia grant 9067-00010B). P.C. and X.Z. were supported by the National Natural Science Foundation of China (Grant Nos 21633011 and 21988101). The material based upon work by A.J.M. and B.M.C. was supported by the National Science Foundation under Grant No. 1943707. I.E.L.S. and J.B. acknowledge financial support from the Engineering and Physical Sciences Research Council (EP/M0138/1), the European Research Council (ERC) under the European Union’s Horizon 2020 research and innovation programme (grant agreement No. 866402) and the National Research Council Canada through the Materials for Clean Fuels Challenge Program. The authors thank M. Hatzell and Z. J. Xu for insightful

discussion regarding N₂ oxidation, and V. Shadravan for helpful advice on thermochemical catalysis. The authors acknowledge J. Montoya for providing data on the vibrational frequencies and free energy calculations for N₂ reduction on Ru(211) for Fig. 9a.

Ethics Declaration

Competing interests

The authors declare no competing interests.

Author Contributions

Introduction (H.I., S.Z.A., A.J.M., and Y. S.-H.); Experimentation (H.I., S.Z.A., X.Z., J.B., P.C., I.E.L.S., I.C., and Y. S.-H.); Results (H.I., S.Z.A., X.Z., B.M.C., J.B., P.C., I.C., A.J.M., and Y. S.-H.); Applications (H.I. and S.Z.A.); Reproducibility and data deposition (H.I. and I.C.); Limitations and optimizations (S.Z.A.); Outlook (H.I., S.Z.A., J.B., X.Z. and I.E.L.S.); Overview of the Primer (H.I., S.Z.A., and Y. S.-H.). All authors discussed and edited the full manuscript.

Priority References

¹¹ Chen, J. G. *et al.* Beyond fossil fuel–driven nitrogen transformations. *Science* (80-.). **360**, eaar6611 (2018): **This review covers the thermochemistry of all nitrogen transformation reactions, and the challenges and opportunities associated with these reactions in overcoming reliance on fossil fuels.**

²⁸ MacFarlane, D. R. *et al.* A Roadmap to the Ammonia Economy. *Joule* **4**, 1186–1205 (2020). **This paper covers 3 different generations of technological advancement needed to produce ammonia sustainably.**

⁶⁹ Medford, A. J. *et al.* From the Sabatier principle to a predictive theory of transition-metal heterogeneous catalysis. *J. Catal.* **328**, 36–42 (2015). **This paper discusses scaling relations, activity maps, and the d-band model, thereby mapping out the development of trends in transition-metal catalysts.**

²⁰⁷ Singh, A. R. *et al.* Electrochemical Ammonia Synthesis—The Selectivity Challenge. *ACS Catal.* **7**, 706–709 (2017): **This viewpoint illucidates the selectivity challenge by covering a qualitative analysis of electrochemical ammonia synthesis and suggests strategies to circumvent the issue.**

⁷³ Montoya, J. H., Tsai, C., Vojvodic, A. & Nørskov, J. K. The Challenge of Electrochemical Ammonia Synthesis: A New Perspective on the Role of Nitrogen Scaling Relations. *ChemSusChem* **8**, 2180–2186 (2015). **This paper presents insights from DFT calculations that describe limitations on the low-temperature electrocatalytic production of ammonia from dinitrogen.**

⁷⁶ Andersen, S. Z. *et al.* A rigorous electrochemical ammonia synthesis protocol with quantitative isotope measurements. *Nature* **570**, 504–508 (2019): **This letter provides a rigorous protocol from which the source of activated nitrogen can be determined.**

⁹⁶ Dabundo, R. *et al.* The Contamination of Commercial ¹⁵N₂ Gas Stocks with ¹⁵N–Labeled Nitrate and Ammonium and Consequences for Nitrogen Fixation Measurements. *PLoS One* **9**, e110335 (2014): **This paper shows that commercial isotope labelled ¹⁵N₂ contains significant contamination across lot numbers and different manufacturers.**

¹⁷⁷ Chen, Y. *et al.* Revealing nitrogen-containing species in commercial catalysts used for ammonia electrosynthesis. *Nat. Catal.* **3**, (2020): **This paper shows that various commercially sold pure metals contain significant N-containing contamination, and provides a way to measure these contaminants.**

¹²¹ Nielander, A. C. *et al.* A Versatile Method for Ammonia Detection in a Range of Relevant Electrolytes via Direct Nuclear Magnetic Resonance Techniques. *ACS Catal.* **9**, 5797–5802 (2019): **This paper reports on a frequency-selective pulse nuclear magnetic resonance method for the accurate determination of ammonia.**

²⁰⁸ Hodgetts, R. Y. *et al.* Refining Universal Procedures for Ammonium Quantification via Rapid ¹ H NMR Analysis for Dinitrogen Reduction Studies. *ACS Energy Lett.* **5**, 736–741 (2020). **This paper assesses the sensitivity of nuclear magnetic resonance towards the detection of ammonia in solutions with different proton concentration**

¹⁰¹ Choi, J. *et al.* Identification and elimination of false positives in electrochemical nitrogen reduction studies. *Nat. Commun.* **11**, 5546 (2020). **This perspective assesses a wide range of electrocatalytic nitrogen reduction reports identifying false positives and providing an experimental protocol for ensuring rigorous ammonia quantification in upcoming works.**

⁷⁸ Wang, P. *et al.* Breaking scaling relations to achieve low-temperature ammonia synthesis through LiH-mediated nitrogen transfer and hydrogenation. *Nat. Chem.* **9**, 64–70 (2017): **This study designed a two-active-center strategy using TM(N)-LiH composite catalysts to create an energy-efficient pathway that allows NH₃ synthesis under mild conditions.**

¹⁵² Holzman, P. R., Shiflett, W. K. & Dumesic, J. A. The importance of ammonia pressure in the kinetics of ammonia synthesis over supported Ru. *J. Catal.* **62**, 167–172 (1980): **This study compared the results of apparent activation energies measured at constant ammonia pressure and at constant flow rate, demonstrating the importance of ammonia partial pressure for reaction kinetics.**

¹⁴⁹ Kojima, R. & Aika, K. Cobalt molybdenum bimetallic nitride catalysts for ammonia synthesis Part 2. Kinetic study.pdf. *Appl. Catal. A Gen.* **218**, 121–128 (2001). **This article presents a typical kinetic study for thermocatalytic ammonia synthesis, including the measurement conditions, derivation process of the equations, and the calculations.**

¹⁶⁵ Núñez, M., Lansford, J. L. & Vlachos, D. G. Optimization of the facet structure of transition-metal catalysts applied to the oxygen reduction reaction. *Nat. Chem.* **11**, 449–456 (2019): **This paper shows trade-offs between activity and stability.**

¹⁶³ Sholl, D. S. & Steckel, J. A. *Density Functional Theory: A Practical Introduction*, Chapter 5, Pg. 113-130. *Density Functional Theory: A Practical Introduction* (2009). **Book chapter covering zero point energy and entropy/enthalpy energy terms, and provides a good overview of the theory.**

References

1. Cottrell, T. L. The Strengths of Chemical Bonds, 2nd Ed. *Prop. atoms, radicals, Bond* (1966).
2. Jia, H.-P. & Quadrelli, E. A. Mechanistic aspects of dinitrogen cleavage and hydrogenation to produce ammonia in catalysis and organometallic chemistry: relevance of metal hydride bonds and dihydrogen. *Chem. Soc. Rev.* **43**, 547–564 (2014).

3. Noxon, J. F. Atmospheric nitrogen fixation by lightning. *Geophys. Res. Lett.* (1976) doi:10.1029/GL003i008p00463.
4. Rivera Ortiz, J. M. & Burris, R. H. Interactions among substrates and inhibitors of nitrogenase. *J. Bacteriol.* (1975) doi:10.1128/jb.123.2.537-545.1975.
5. Yang, Z. Y. *et al.* Evidence That the Pi Release Event Is the Rate-Limiting Step in the Nitrogenase Catalytic Cycle. *Biochemistry* (2016) doi:10.1021/acs.biochem.6b00421.
6. Hoffman, B. M., Lukyanov, D., Yang, Z., Dean, D. R. & Seefeldt, L. C. Mechanism of Nitrogen Fixation by Nitrogenase: The Next Stage. *Chem. Rev.* **114**, 4041–4062 (2014).
7. Smil, V. *Enriching the Earth: Fritz Haber, Carl Bosch, and the Transformation of World Food Production.* (The MIT Press, 2001).
8. Hager, T. *The Alchemy of Air: A Jewish Genius, a Doomed Tycoon, and the Discovery that Changed the Course of History.* Broadway Books (Broadway Books, 2008).
9. Science and Food Supplies. *Nature* **126**, 193–194 (1930).
10. Ihde, A. J. *The Development of Modern Chemistry (Dover Books on Chemistry).* (Dover Publications, 1984).
11. Chen, J. G. *et al.* Beyond fossil fuel–driven nitrogen transformations. *Science (80-).* **360**, eaar6611 (2018).
12. Smith, C., Hill, A. K. & Torrente-Murciano, L. Current and future role of Haber–Bosch ammonia in a carbon-free energy landscape. *Energy Environ. Sci.* (2020) doi:10.1039/C9EE02873K.
13. Aika, K. & Tamara, K. Ammonia Synthesis over Non-Iron Catalysts and Related Phenomena. in *Ammonia* (1995). doi:10.1007/978-3-642-79197-0_3.
14. Ertl, G. Reactions at Surfaces: From Atoms to Complexity (Nobel Lecture). *Angew. Chemie Int. Ed.* **47**, 3524–3535 (2008).
15. Erisman, J. W., Sutton, M. a., Galloway, J., Klimont, Z. & Winiwarter, W. How a century of ammonia synthesis changed the world. *Nat. Geosci.* **1**, 636–639 (2008).
16. Smil, V. Nitrogen and Food Production: Proteins for Human Diets. *AMBIO A J. Hum. Environ.* **31**, 126–131 (2002).
17. Stewart, W. M., Dibb, D. W., Johnston, A. E. & Smyth, T. J. The Contribution of Commercial Fertilizer Nutrients to Food Production. *Agron. J.* **97**, 1–6 (2005).
18. USGS National Minerals Information Center. *Nitrogen Statistics and Information, U.S. Geological Survey, Mineral Commodity Summaries, January 2020.* <https://www.usgs.gov/centers/nmic/nitrogen-statistics-and-information> (2020).
19. Apodaca, L. E. Nitrogen (fixed) — Ammonia. 116–117 (2019).
20. Smil, V. Detonator of the population explosion. *Nature* **400**, 415–415 (1999).
21. Schlägl, R. Ammonia Synthesis. in *Handbook of Heterogeneous Catalysis* 2501 (Wiley-VCH Verlag GmbH & Co. KGaA, 2008). doi:10.1002/9783527610044.hetcat0129.
22. IHS Markit. *Ammonia - Chemical Economics Handbook (CEH) | IHS Markit.* [IHSmarkit.com](https://ihsmarkit.com/products/ammonia-chemical-economics-handbook.html) (2020).
23. Klerke, A., Christensen, C. H., Nørskov, J. K. & Vegge, T. Ammonia for hydrogen storage:

challenges and opportunities. *J. Mater. Chem.* **18**, 2304 (2008).

- 24. Zamfirescu, C. & Dincer, I. Using ammonia as a sustainable fuel. *J. Power Sources* **185**, 459–465 (2008).
- 25. Brightling, J. Ammonia and the Fertiliser Industry: The Development of Ammonia at Billingham A history of technological innovation from the early 20th century to the present day. *Johnson Matthey Technol. Rev.* (2018).
- 26. Brown, T. Ammonia production causes 1% of total global GHG emissions. <https://ammoniaindustry.com/ammonia-production-causes-1-percent-of-total-global-ghg-emissions/>.
- 27. Soloveichik, G. Electrochemical synthesis of ammonia as a potential alternative to the Haber–Bosch process. *Nature Catalysis* (2019) doi:10.1038/s41929-019-0280-0.
- 28. MacFarlane, D. R. *et al.* A Roadmap to the Ammonia Economy. *Joule* **4**, 1186–1205 (2020).
- 29. Smith, C., Hill, A. K. & Torrente-Murciano, L. Current and future role of Haber-Bosch ammonia in a carbon-free energy landscape. *Energy Environ. Sci.* **13**, 331–344 (2020).
- 30. Stephens, I. & Nilsson, A. Research needs towards sustainable production of fuels and chemicals. *Energy-X, Chapter 5* <https://www.energy-x.eu/research-needs-report/> (2019).
- 31. Erisman, J. W., Bleeker, A., Galloway, J. & Sutton, M. S. Reduced nitrogen in ecology and the environment. *Environ. Pollut.* **150**, 140–149 (2007).
- 32. Good, A. G. & Beatty, P. H. Fertilizing nature: A tragedy of excess in the commons. *PLoS Biol.* **9**, 1–9 (2011).
- 33. Singh, A. R. *et al.* Electrochemical Ammonia Synthesis - The Selectivity Challenge. *ACS Catalysis* (2017) doi:10.1021/acscatal.6b03035.
- 34. Comer, B. M. *et al.* Prospects and Challenges for Solar Fertilizers. *Joule* (2019) doi:10.1016/j.joule.2019.05.001.
- 35. Ummary, S. Renewable Energy to Fuels Through Utilization of EnergyDense Liquids (REFUEL) Program Overview. 1–16 (2016).
- 36. Rouwenhorst, K. H. R., Kim, H. H. & Lefferts, L. vibrationally Excited Activation of N2 in Plasma-Enhanced Catalytic Ammonia Synthesis: A Kinetic Analysis. *ACS Sustain. Chem. Eng.* (2019) doi:10.1021/acssuschemeng.9b04997.
- 37. Rouwenhorst, K. H. R. *et al.* Plasma-driven catalysis: Green ammonia synthesis with intermittent electricity. *Green Chem.* (2020) doi:10.1039/d0gc02058c.
- 38. Kim, H. H., Teramoto, Y., Ogata, A., Takagi, H. & Nanba, T. Atmospheric-pressure nonthermal plasma synthesis of ammonia over ruthenium catalysts. *Plasma Process. Polym.* (2017) doi:10.1002/ppap.201600157.
- 39. Mehta, P. *et al.* Overcoming ammonia synthesis scaling relations with plasma-enabled catalysis. *Nat. Catal.* (2018) doi:10.1038/s41929-018-0045-1.
- 40. Han, G.-F. *et al.* Mechanochemistry for ammonia synthesis under mild conditions. *Nat. Nanotechnol.* **Accepted**, (2020).
- 41. Tricker, A. W. *et al.* Mechanocatalytic Ammonia Synthesis over TiN in Transient Microenvironments. *ACS Energy Lett.* **5**, 3362–3367 (2020).

42. IHS. Chemical Economics Handbooks (CEH) | IHS. *IHS, 15. October* (2015).

43. Bard, a & Faulkner, L. Chapter 2, *Electrochemical Methods: Fundamentals and Applications*, New York: , 2001. *Russ. J. Electrochem.* (2002).

44. Birkeland, K. R. On the oxidation of atmospheric nitrogen in electric arcs. *Trans. Faraday Soc.* (1906) doi:10.1039/tf9060200098.

45. Eyde, S. Oxidation of atmospheric nitrogen and development of resulting industries in norway. *Ind. Eng. Chem.* (1912) doi:10.1021/ie50046a025.

46. Cherkasov, N., Ibhadon, A. O. & Fitzpatrick, P. A review of the existing and alternative methods for greener nitrogen fixation. *Chemical Engineering and Processing: Process Intensification* (2015) doi:10.1016/j.cep.2015.02.004.

47. Hessel, V. *et al.* Industrial applications of plasma, microwave and ultrasound techniques: Nitrogen-fixation and hydrogenation reactions. *Chem. Eng. Process. Process Intensif.* (2013) doi:10.1016/j.cep.2013.02.002.

48. Rusanov, V. D., Fridman, A. A. & Sholin, G. V. The Physics of a Chemically Active Plasma With Nonequilibrium Vibrational Excitationc of Molecules. *Sov. Phys. - Uspekhi* (1981) doi:10.1070/PU1981v024n06ABEH004884.

49. Li, S., Medrano, J. A., Hessel, V. & Gallucci, F. Recent progress of plasma-assisted nitrogen fixation research: A review. *Processes* (2018) doi:10.3390/pr6120248.

50. Dai, C., Sun, Y., Chen, G., Fisher, A. C. & Xu, Z. J. Electrochemical Oxidation of Nitrogen towards Direct Nitrate Production on Spinel Oxides. *Angew. Chemie Int. Ed.* **59**, 9418–9422 (2020).

51. Fang, W. *et al.* Boosting efficient ambient nitrogen oxidation by a well-dispersed Pd on MXene electrocatalyst. *Chem. Commun.* **56**, 5779–5782 (2020).

52. Wang, Y., Yu, Y., Jia, R., Zhang, C. & Zhang, B. Electrochemical synthesis of nitric acid from air and ammonia through waste utilization. *Natl. Sci. Rev.* **6**, 730–738 (2019).

53. Lun Pang, C., Lindsay, R. & Thornton, G. Chemical reactions on rutile TiO₂(110). *Chem. Soc. Rev.* (2008) doi:10.1039/b719085a.

54. Bickley, R. I. & Vishwanathan, V. Photocatalytically induced fixation of molecular nitrogen by near UV radiation [6]. *Nature* (1979) doi:10.1038/280306a0.

55. Yuan, S. J. *et al.* Nitrate formation from atmospheric nitrogen and oxygen photocatalysed by nano-sized titanium dioxide. *Nat. Commun.* (2013) doi:10.1038/ncomms3249.

56. Kuang, M. *et al.* Efficient Nitrate Synthesis via Ambient Nitrogen Oxidation with Ru-Doped TiO₂/RuO₂ Electrocatalysts. *Adv. Mater.* **32**, 2002189 (2020).

57. Wang, S. *et al.* Universal transition state scaling relations for (de)hydrogenation over transition metals. *Phys. Chem. Chem. Phys.* (2011) doi:10.1039/c1cp20547a.

58. Bozso, F., Ertl, G., Grunze, M. & Weiss, M. Interaction of nitrogen with iron surfaces. I. Fe(100) and Fe(111). *J. Catal.* (1977) doi:10.1016/0021-9517(77)90237-8.

59. Bozso, F., Ertl, G. & Weiss, M. Interaction of nitrogen with iron surfaces. II. Fe(110). *J. Catal.* (1977) doi:10.1016/0021-9517(77)90063-X.

60. Ertl, G., Lee, S. B. & Weiss, M. Adsorption of nitrogen on potassium promoted Fe(111) and (100) surfaces. *Surf. Sci.* (1982) doi:10.1016/0039-6028(82)90703-8.

61. Honkala, K. *et al.* Ammonia synthesis from first-principles calculations. *Science* (80-.). (2005) doi:10.1126/science.1106435.

62. Dahl, S. *et al.* Role of steps in N₂ activation on Ru(0001). *Phys. Rev. Lett.* (1999) doi:10.1103/PhysRevLett.83.1814.

63. Chorkendorff, I. & Niemantsverdriet, J. W. Reaction Rate Theory. in *Concepts of Modern Catalysis and Kinetics* (2003). doi:10.1002/3527602658.ch3.

64. Medford, A. J. & Hatzell, M. C. Photon-Driven Nitrogen Fixation: Current Progress, Thermodynamic Considerations, and Future Outlook. *ACS Catal.* **7**, 2624–2643 (2017).

65. Comer, B. M. & Medford, A. J. Analysis of Photocatalytic Nitrogen Fixation on Rutile TiO₂(110). *ACS Sustain. Chem. Eng.* **6**, 4648–4660 (2018).

66. Singh, A. R. *et al.* Strategies toward Selective Electrochemical Ammonia Synthesis. *ACS Catal.* **9**, 8316–8324 (2019).

67. Medford, A. J. *et al.* Assessing the reliability of calculated catalytic ammonia synthesis rates. *Science* (80-.). (2014) doi:10.1126/science.1253486.

68. Wellendorff, J. *et al.* Density functionals for surface science: Exchange-correlation model development with Bayesian error estimation. *Phys. Rev. B - Condens. Matter Mater. Phys.* (2012) doi:10.1103/PhysRevB.85.235149.

69. Medford, A. J. *et al.* From the Sabatier principle to a predictive theory of transition-metal heterogeneous catalysis. *J. Catal.* **328**, 36–42 (2015).

70. Bare, S. R., Strongin, D. R. & Somorjai, G. A. Ammonia synthesis over iron single-crystal catalysts: The effects of alumina and potassium. *J. Phys. Chem.* (1986) doi:10.1021/j100411a003.

71. Dahl, S., Taylor, P. A., Törnqvist, E. & Chorkendorff, I. The synthesis of ammonia over a ruthenium single crystal. *J. Catal.* (1998) doi:10.1006/jcat.1998.2168.

72. Singh, A. R. *et al.* Computational Design of Active Site Structures with Improved Transition-State Scaling for Ammonia Synthesis. *ACS Catal.* (2018) doi:10.1021/acscatal.8b00106.

73. Montoya, J. H., Tsai, C., Vojvodic, A. & Nørskov, J. K. The challenge of electrochemical ammonia synthesis: A new perspective on the role of nitrogen scaling relations. *ChemSusChem* (2015) doi:10.1002/cssc.201500322.

74. Skúlason, E. *et al.* A theoretical evaluation of possible transition metal electro-catalysts for N₂ reduction. *Phys. Chem. Chem. Phys.* (2012) doi:10.1039/c1cp22271f.

75. Rostamikia, G., Maheshwari, S. & Janik, M. J. Elementary kinetics of nitrogen electroreduction to ammonia on late transition metals. *Catal. Sci. Technol.* (2019) doi:10.1039/c8cy01845f.

76. Andersen, S. Z. *et al.* A rigorous electrochemical ammonia synthesis protocol with quantitative isotope measurements. *Nature* **570**, 504–508 (2019).

77. Suryanto, B. H. R. *et al.* Challenges and prospects in the catalysis of electroreduction of nitrogen to ammonia. *Nat. Catal.* **2**, 290–296 (2019).

78. Wang, P. *et al.* Breaking scaling relations to achieve low-temperature ammonia synthesis through LiH-mediated nitrogen transfer and hydrogenation. *Nat. Chem.* **9**, 64–70 (2017).

79. Schwalbe, J. A. *et al.* A Combined Theory-Experiment Analysis of the Surface Species in Lithium-Mediated NH₃ Electrosynthesis. *ChemElectroChem* **7**, 1542–1549 (2020).

80. Lazouski, N., Chung, M., Williams, K., Gala, M. L. & Manthiram, K. Non-aqueous gas diffusion electrodes for rapid ammonia synthesis from nitrogen and water-splitting-derived hydrogen. *Nat. Catal.* **3**, 463–469 (2020).

81. Lazouski, N., Schiffer, Z. J., Williams, K. & Manthiram, K. Understanding Continuous Lithium-Mediated Electrochemical Nitrogen Reduction. *Joule* (2019) doi:10.1016/j.joule.2019.02.003.

82. Andersen, S. Z. *et al.* Increasing stability, efficiency, and fundamental understanding of lithium-mediated electrochemical nitrogen reduction. *Energy Environ. Sci.* (2020) doi:10.1039/D0EE02246B.

83. McEnaney, J. M. *et al.* Ammonia synthesis from N₂ and H₂O using a lithium cycling electrification strategy at atmospheric pressure. *Energy Environ. Sci.* (2017) doi:10.1039/c7ee01126a.

84. Kim, K. *et al.* Lithium-Mediated Ammonia Electro-Synthesis: Effect of CsClO₄ on Lithium Plating Efficiency and Ammonia Synthesis. *J. Electrochem. Soc.* (2018) doi:10.1149/2.1091811jes.

85. Hattori, M., Iijima, S., Nakao, T., Hosono, H. & Hara, M. Solid solution for catalytic ammonia synthesis from nitrogen and hydrogen gases at 50 °C. *Nat. Commun.* (2020) doi:10.1038/s41467-020-15868-8.

86. Davy, H. The Bakerian Lecture, on some chemical agencies of electricity. *Philos. Trans. R. Soc. London* **97**, 1–56 (1807).

87. Rayleigh, Lord. XIII.—Observations on the oxidation of nitrogen gas. *J. Chem. Soc., Trans.* **71**, 181–186 (1897).

88. Boucher, D. L., Davies, J. A., Edwards, J. G. & Mennad, A. An investigation of the putative photosynthesis of ammonia on iron-doped titania and other metal oxides. *J. Photochem. Photobiol. A Chem.* **88**, 53–64 (1995).

89. Shipman, M. A. & Symes, M. D. A re-evaluation of Sn(II) phthalocyanine as a catalyst for the electrosynthesis of ammonia. *Electrochim. Acta* **258**, 618–622 (2017).

90. Du, H.-L., Gengenbach, T. R., Hodgetts, R., MacFarlane, D. R. & Simonov, A. N. Critical Assessment of the Electrocatalytic Activity of Vanadium and Niobium Nitrides toward Dinitrogen Reduction to Ammonia. *ACS Sustain. Chem. Eng.* **7**, 6839–6850 (2019).

91. Choi, J. *et al.* Promoting nitrogen electroreduction to ammonia with bismuth nanocrystals and potassium cations in water. *ChemRxiv, Prepr.* (2020).

92. Yang, X. *et al.* Quantification of Active Sites and Elucidation of the Reaction Mechanism of the Electrochemical Nitrogen Reduction Reaction on Vanadium Nitride. *Angew. Chemie* **131**, 13906–13910 (2019).

93. Bao, D. *et al.* Electrochemical Reduction of N₂ under Ambient Conditions for Artificial N₂ Fixation and Renewable Energy Storage Using N₂/NH₃ Cycle. *Adv. Mater.* **29**, 1604799 (2017).

94. Hao, Y.-C. *et al.* Promoting nitrogen electroreduction to ammonia with bismuth nanocrystals and potassium cations in water. *Nat. Catal.* **2**, 448–456 (2019).

95. Smeets, M. A. M. *et al.* Odor and Irritation Thresholds for Ammonia: A Comparison between Static and Dynamic Olfactometry. *Chem. Senses* **32**, 11–20 (2007).

96. Dabundo, R. *et al.* The Contamination of Commercial ¹⁵N₂ Gas Stocks with ¹⁵N–Labeled Nitrate and Ammonium and Consequences for Nitrogen Fixation Measurements. *PLoS One* **9**, e110335

(2014).

97. Giordano, L. *et al.* PH dependence of OER activity of oxides: Current and future perspectives. *Catal. Today* **262**, 2–10 (2016).
98. Shinagawa, T., Garcia-Esparza, A. T. & Takanabe, K. Insight on Tafel slopes from a microkinetic analysis of aqueous electrocatalysis for energy conversion. *Sci. Rep.* **5**, 13801 (2015).
99. Limaye, A., Zeng, J. S., Willard, A. & Manthiram, K. Bayesian Data Analysis Reveals No Preference for Cardinal Tafel Slopes in CO₂ Reduction Electrocatalysis. *ChemRxiv* (2020) doi:10.26434/chemrxiv.12844715.v1.
100. Neyerlin, K. C., Gu, W., Jorne, J. & Gasteiger, H. A. Determination of Catalyst Unique Parameters for the Oxygen Reduction Reaction in a PEMFC. *J. Electrochem. Soc.* **153**, A1955 (2006).
101. Choi, J. *et al.* Identification and elimination of false positives in electrochemical nitrogen reduction studies. *Nat. Commun.* **11**, 5546 (2020).
102. Wei, C. *et al.* Recommended Practices and Benchmark Activity for Hydrogen and Oxygen Electrocatalysis in Water Splitting and Fuel Cells. *Adv. Mater.* **31**, 1806296 (2019).
103. Ledezma-Yanez, I., Díaz-Morales, O., Figueiredo, M. C. & Koper, M. T. M. Hydrogen Oxidation and Hydrogen Evolution on a Platinum Electrode in Acetonitrile. *ChemElectroChem* **2**, 1612–1622 (2015).
104. Raccichini, R., Amores, M. & Hinds, G. Critical review of the use of reference electrodes in li-ion batteries: A diagnostic perspective. *Batteries* (2019) doi:10.3390/batteries5010012.
105. Ren, Y. *et al.* Is It Appropriate to Use the Nafion Membrane in Electrocatalytic N₂ Reduction? *Small Methods* **3**, 1900474 (2019).
106. Liu, H., Zhang, Y. & Luo, J. The removal of inevitable NO species in catalysts and the selection of appropriate membrane for measuring electrocatalytic ammonia synthesis accurately. *J. Energy Chem.* **49**, 51–58 (2020).
107. Hongsirikarn, K., Goodwin, J. G., Greenway, S. & Creager, S. Influence of ammonia on the conductivity of Nafion membranes. *J. Power Sources* **195**, 30–38 (2010).
108. Halseid, R., Vie, P. J. S. & Tunold, R. Influence of Ammonium on Conductivity and Water Content of Nafion 117 Membranes. *J. Electrochem. Soc.* **151**, A381 (2004).
109. Lindley, B. M., Appel, A. M., Krogh-Jespersen, K., Mayer, J. M. & Miller, A. J. M. Evaluating the Thermodynamics of Electrocatalytic N₂ Reduction in Acetonitrile. *ACS Energy Lett.* (2016) doi:10.1021/acsenergylett.6b00319.
110. Guo, J. *et al.* Lithium imide synergy with 3d transition-metal nitrides leading to unprecedented catalytic activities for ammonia decomposition. *Angew. Chemie, Int. Ed. English* **54**, 2950–2954 (2015).
111. Kitano, M. *et al.* Ammonia synthesis using a stable electrode as an electron donor and reversible hydrogen store. *Nat. Chem.* **4**, 934–940 (2012).
112. Ma, Z., Zhao, S., Pei, X., Xiong, X. & Hu, B. New insights into the support morphology-dependent ammonia synthesis activity of Ru/CeO₂ catalysts. *Catal. Sci. Technol.* **7**, 191–199 (2017).
113. Wu, S. *et al.* Removal of Hydrogen Poisoning by Electrostatically Polar MgO Support for Low-

Pressure NH₃ Synthesis at a High Rate over the Ru Catalyst. *ACS Catal.* **10**, 5614–5622 (2020).

- 114. Searle, P. L. The berthelot or indophenol reaction and its use in the analytical chemistry of nitrogen. A review. *Analyst* **109**, 549 (1984).
- 115. Zhao, Y. *et al.* Ammonia Detection Methods in Photocatalytic and Electrocatalytic Experiments: How to Improve the Reliability of NH₃ Production Rates? *Adv. Sci.* **6**, 1802109 (2019).
- 116. Zhou, L. & Boyd, C. E. Comparison of Nessler, phenate, salicylate and ion selective electrode procedures for determination of total ammonia nitrogen in aquaculture. *Aquaculture* **450**, 187–193 (2016).
- 117. Giner-Sanz, J. J., Leverick, G. M., Pérez-Herranz, V. & Shao-Horn, Y. Salicylate Method for Ammonia Quantification in Nitrogen Electroreduction Experiments: The Correction of Iron III Interference. *J. Electrochem. Soc.* (2020) doi:10.1149/1945-7111/abbdd6.
- 118. Murray, E. *et al.* A colorimetric method for use within portable test kits for nitrate determination in various water matrices. *Anal. Methods* **9**, 680–687 (2017).
- 119. Hayashi, M. Temperature-electrical conductivity relation of water for environmental monitoring and geophysical data inversion. *Environ. Monit. Assess.* **96**, 119–128 (2004).
- 120. Bruker. What Is NMR? *Bruker BioSpin* 145–158 (2010) doi:10.1201/b15748-14.
- 121. Nielander, A. C. *et al.* A Versatile Method for Ammonia Detection in a Range of Relevant Electrolytes via Direct Nuclear Magnetic Resonance Techniques. *ACS Catal.* **9**, 5797–5802 (2019).
- 122. Mooney, E. F. & Winson, P. H. Nitrogen Magnetic Resonance Spectroscopy. *Annu. Reports NMR Spectrosc.* **2**, 125–152 (1969).
- 123. Giddey, S., Badwal, S. P. S. & Kulkarni, A. Review of electrochemical ammonia production technologies and materials. *Int. J. Hydrogen Energy* **38**, 14576–14594 (2013).
- 124. Seh, Z. W. *et al.* Combining theory and experiment in electrocatalysis: Insights into materials design. *Science (80-.).* **355**, eaad4998 (2017).
- 125. Choi, J. *et al.* Electroreduction of Nitrates, Nitrites, and Gaseous Nitrogen Oxides: A Potential Source of Ammonia in Dinitrogen Reduction Studies. *ACS Energy Lett.* **5**, 2095–2097 (2020).
- 126. Li, J. & Wu, N. Semiconductor-based photocatalysts and photoelectrochemical cells for solar fuel generation: A review. *Catalysis Science and Technology* (2015) doi:10.1039/c4cy00974f.
- 127. Kisch, H. Semiconductor Photocatalysis-Mechanistic and Synthetic Aspects. *Angew. Chemie Int. Ed.* **52**, 812–847 (2013).
- 128. Chen, X., Shen, S., Guo, L. & Mao, S. S. Semiconductor-based Photocatalytic Hydrogen Generation. *Chem. Rev.* **110**, 6503–6570 (2010).
- 129. Kibsgaard, J., Nørskov, J. K. & Chorkendorff, I. The Difficulty of Proving Electrochemical Ammonia Synthesis. *ACS Energy Lett.* **4**, 2986–2988 (2019).
- 130. Turner, C., Španěl, P. & Smith, D. A longitudinal study of ammonia, acetone and propanol in the exhaled breath of 30 subjects using selected ion flow tube mass spectrometry, SIFT-MS. *Physiol. Meas.* **27**, 321–337 (2006).
- 131. Tao, H. *et al.* Nitrogen Fixation by Ru Single-Atom Electrocatalytic Reduction. *Chem* **5**, 204–214 (2019).

132. Xiong, W. *et al.* Facile, cost-effective plasma synthesis of self-supportive FeS x on Fe foam for efficient electrochemical reduction of N 2 under ambient conditions. *J. Mater. Chem. A* **7**, 19977–19983 (2019).

133. Suryanto, B. H. R. *et al.* MoS 2 Polymorphic Engineering Enhances Selectivity in the Electrochemical Reduction of Nitrogen to Ammonia. *ACS Energy Lett.* **4**, 430–435 (2019).

134. Li, X. *et al.* Boosted Electrocatalytic N2 Reduction to NH3 by Defect-Rich MoS2 Nanoflower. *Adv. Energy Mater.* **8**, (2018).

135. Chen, G.-F. *et al.* Ammonia Electrosynthesis with High Selectivity under Ambient Conditions via a Li⁺ Incorporation Strategy. *J. Am. Chem. Soc.* **139**, 9771–9774 (2017).

136. Song, Y. *et al.* A physical catalyst for the electrolysis of nitrogen to ammonia. *Sci. Adv.* **4**, e1700336 (2018).

137. Zhou, F. *et al.* Electro-synthesis of ammonia from nitrogen at ambient temperature and pressure in ionic liquids. *Energy Environ. Sci.* **10**, 2516–2520 (2017).

138. Tsuneto, A., Kudo, A. & Sakata, T. Lithium-mediated electrochemical reduction of high pressure N2 to NH3. *J. Electroanal. Chem.* **367**, 183–188 (1994).

139. Tsuneto, A., Kudo, A. & Sakata, T. Efficient Electrochemical Reduction of N2 to NH3 Catalyzed by Lithium. *Chem. Lett.* **22**, 851–854 (1993).

140. Zhang, L. *et al.* A Janus Fe-SnO 2 Catalyst that Enables Bifunctional Electrochemical Nitrogen Fixation. *Angew. Chemie Int. Ed.* **59**, 10888–10893 (2020).

141. Hirakawa, H., Hashimoto, M., Shiraishi, Y. & Hirai, T. Photocatalytic Conversion of Nitrogen to Ammonia with Water on Surface Oxygen Vacancies of Titanium Dioxide. *J. Am. Chem. Soc.* (2017) doi:10.1021/jacs.7b06634.

142. Comer, B. M. *et al.* The Role of Adventitious Carbon in Photo-catalytic Nitrogen Fixation by Titania. *J. Am. Chem. Soc.* (2018) doi:10.1021/jacs.8b08464.

143. Wang, Z. *et al.* Recent Developments in Polymeric Carbon Nitride-Derived Photocatalysts and Electrocatalysts for Nitrogen Fixation. *ACS Catalysis* (2019) doi:10.1021/acscatal.9b03015.

144. Lv, C. *et al.* Defect Engineering Metal-Free Polymeric Carbon Nitride Electrocatalyst for Effective Nitrogen Fixation under Ambient Conditions. *Angew. Chemie - Int. Ed.* (2018) doi:10.1002/anie.201806386.

145. Hu, B., Hu, M., Seefeldt, L. & Liu, T. L. Electrochemical Dinitrogen Reduction to Ammonia by Mo2N: Catalysis or Decomposition? *ACS Energy Lett.* (2019) doi:10.1021/acsenergylett.9b00648.

146. Liu, Q. *et al.* Photocatalytic N2 reduction: Uncertainties in the determination of ammonia production. *ACS Sustain. Chem. Eng.* (2021) doi:10.1021/acssuschemeng.0c08064.

147. Bielawa, H., Hinrichsen, O., Birkner, A. & Muhler, M. The ammonia-synthesis catalyst of the next generation: Barium-promoted oxide-supported ruthenium. *Angew. Chemie-International Ed.* **40**, 1061–+ (2001).

148. Hagen, S. *et al.* New efficient catalyst for ammonia synthesis: barium-promoted cobalt on carbon. *Chem. Commun.* **11**, 1206–1207 (2002).

149. Kojima, R. & Aika, K. Cobalt molybdenum bimetallic nitride catalysts for ammonia synthesis Part 2. Kinetic study.pdf. *Appl. Catal. A Gen.* **218**, 121–128 (2001).

150. Hagen, S. Ammonia synthesis with barium-promoted iron–cobalt alloys supported on carbon. *J.*

Catal. **214**, 327–335 (2003).

151. Aika, K. Role of alkali promoter in ammonia synthesis over ruthenium catalysts—Effect on reaction mechanism. *Catal. Today* **286**, 14–20 (2017).
152. Holzman, P. R., Shiflett, W. K. & Dumesic, J. A. The importance of ammonia pressure in the kinetics of ammonia synthesis over supported Ru. *J. Catal.* **62**, 167–172 (1980).
153. Ye, T.-N. *et al.* Vacancy-enabled N₂ activation for ammonia synthesis on an Ni-loaded catalyst. *Nature* **583**, 391–395 (2020).
154. Tang, Y. *et al.* Metal-Dependent Support Effects of Oxyhydride-Supported Ru, Fe, Co Catalysts for Ammonia Synthesis. *Adv. Energy Mater.* (2018) doi:10.1002/aenm.201801772.
155. Kobayashi, Y. *et al.* Titanium-Based Hydrides as Heterogeneous Catalysts for Ammonia Synthesis. *J. Am. Chem. Soc.* (2017) doi:10.1021/jacs.7b08891.
156. Cao, Y. *et al.* Vanadium Hydride as an Ammonia Synthesis Catalyst. *ChemCatChem* (2020) doi:10.1002/cetc.202001084.
157. Kammert, J. *et al.* Nature of Reactive Hydrogen for Ammonia Synthesis over a Ru/C₁₂A₇ Electride Catalyst. *J. Am. Chem. Soc.* **142**, 7655–7667 (2020).
158. Gao, W., Guo, J. & Chen, P. Hydrides, Amides and Imides Mediated Ammonia Synthesis and Decomposition. *Chinese J. Chem.* **37**, 442–451 (2019).
159. Peterson, A. A., Abild-Pedersen, F., Studt, F., Rossmeisl, J. & Nørskov, J. K. How copper catalyzes the electroreduction of carbon dioxide into hydrocarbon fuels. *Energy Environ. Sci.* (2010) doi:10.1039/c0ee00071j.
160. Sundararaman, R., Goddard, W. A. & Arias, T. A. Grand canonical electronic density-functional theory: Algorithms and applications to electrochemistry. *J. Chem. Phys.* (2017) doi:10.1063/1.4978411.
161. Kastlunger, G., Lindgren, P. & Peterson, A. A. Controlled-Potential Simulation of Elementary Electrochemical Reactions: Proton Discharge on Metal Surfaces. *J. Phys. Chem. C* (2018) doi:10.1021/acs.jpcc.8b02465.
162. Govender, A., Curulla Ferré, D. & Niemantsverdriet, J. W. A density functional theory study on the effect of zero-point energy corrections on the methanation profile on Fe(100). *ChemPhysChem* (2012) doi:10.1002/cphc.201100733.
163. Sholl, D. S. & Steckel, J. A. *Density Functional Theory: A Practical Introduction, Chapter 5, Pg. 113-130. Density Functional Theory: A Practical Introduction* (2009). doi:10.1002/9780470447710.
164. Sprowl, L. H., Campbell, C. T. & Árnadóttir, L. Hindered translator and hindered rotor models for adsorbates: Partition functions and entropies. *J. Phys. Chem. C* (2016) doi:10.1021/acs.jpcc.5b11616.
165. Núñez, M., Lansford, J. L. & Vlachos, D. G. Optimization of the facet structure of transition-metal catalysts applied to the oxygen reduction reaction. *Nat. Chem.* (2019) doi:10.1038/s41557-019-0247-4.
166. Goldsmith, B. R., Sanderson, E. D., Bean, D. & Peters, B. Isolated catalyst sites on amorphous supports: A systematic algorithm for understanding heterogeneities in structure and reactivity. *J. Chem. Phys.* (2013) doi:10.1063/1.4807384.

167. Wexler, R. B., Qiu, T. & Rappe, A. M. Automatic Prediction of Surface Phase Diagrams Using Ab Initio Grand Canonical Monte Carlo. *J. Phys. Chem. C* (2019) doi:10.1021/acs.jpcc.8b11093.

168. Shimanouchi, T. ‘Molecular Vibrational Frequencies’ in NIST Chemistry WebBook. *NIST Standard Reference Database Number 69* <https://doi.org/10.18434/T4D303>.

169. Service, R. F. Liquid Sunshine. *Science (80-.)*. **361**, 120–123 (2018).

170. Christensen, C. H., Johannessen, T., Sørensen, R. Z. & Nørskov, J. K. Towards an ammonia-mediated hydrogen economy? *Catal. Today* **111**, 140–144 (2006).

171. Soloveichik, G. ARPA-E REFUEL Program: Distributed Production of Ammonia and its Conversion to Energy. in *2019 AIChE Annual Meeting* (AIChE, 2019).

172. Nielander, A. C. *et al.* Readily Constructed Glass Piston Pump for Gas Recirculation. *ACS Omega* **5**, 16455–16459 (2020).

173. Tang, C. & Qiao, S.-Z. How to explore ambient electrocatalytic nitrogen reduction reliably and insightfully. *Chem. Soc. Rev.* **48**, 3166–3180 (2019).

174. Shi, R., Zhang, X., Waterhouse, G. I. N., Zhao, Y. & Zhang, T. The Journey toward Low Temperature, Low Pressure Catalytic Nitrogen Fixation. *Adv. Energy Mater.* **10**, (2020).

175. Munter, T. R., Bligaard, T., Christensen, C. H. & Nørskov, J. K. BEP relations for N₂ dissociation over stepped transition metal and alloy surfaces. *Phys. Chem. Chem. Phys.* **10**, 5202–5206 (2008).

176. Yu, W. *et al.* Cathodic NH₄⁺ leaching of nitrogen impurities in CoMo thin-film electrodes in aqueous acidic solutions. *Sustain. Energy Fuels* **4**, 5080–5087 (2020).

177. Chen, Y. *et al.* Revealing nitrogen-containing species in commercial catalysts used for ammonia electrosynthesis. *Nat. Catal.* **3**, (2020).

178. Hargreaves, J. S. J. Heterogeneous catalysis with metal nitrides. *Coordination Chemistry Reviews* (2013) doi:10.1016/j.ccr.2012.10.005.

179. Krauth, O., Fahsold, G. & Lehmann, A. Surface-enhanced infrared absorption. *Surf. Sci.* **433**, 79–82 (1999).

180. Yao, Y., Zhu, S., Wang, H., Li, H. & Shao, M. A Spectroscopic Study on the Nitrogen Electrochemical Reduction Reaction on Gold and Platinum Surfaces. *J. Am. Chem. Soc.* **140**, 1496–1501 (2018).

181. Yao, Y., Wang, H., Yuan, X. Z., Li, H. & Shao, M. Electrochemical Nitrogen Reduction Reaction on Ruthenium. *ACS Energy Lett.* **4**, 1336–1341 (2019).

182. Matsui, T. *et al.* In Situ Attenuated Total Reflection Infrared Spectroscopy on Electrochemical Ammonia Oxidation over Pt Electrode in Alkaline Aqueous Solutions. *Langmuir* **31**, 11717–11723 (2015).

183. Abdiaziz, K., Salvadori, E., Sokol, K. P., Reisner, E. & Roessler, M. M. Protein film electrochemical EPR spectroscopy as a technique to investigate redox reactions in biomolecules. *Chem. Commun.* **55**, 8840–8843 (2019).

184. Bajada, M. A. *et al.* A Precious-Metal-Free Hybrid Electrolyzer for Alcohol Oxidation Coupled to CO₂-to-Syngas Conversion. *Angew. Chemie Int. Ed.* **59**, 15633–15641 (2020).

185. Joris, G. G. & Taylor, H. S. Exchange reactions of nitrogen isotopes on iron and tungsten surfaces. *J. Chem. Phys.* **7**, 893–898 (1939).

186. Urabe, K. Activation of nitrogen by alkali metal-promoted transition metal II. Isotopic exchange in molecular nitrogen over potassium-promoted ruthenium-carbon catalyst. *J. Catal.* **32**, 108–113 (1974).

187. Urabe, K. Activation of nitrogen by alkali metal-promoted transition metal VI. Hydrogen effect on isotopic equilibration of nitrogen and rate-determining step of ammonia synthesis on potassium-promoted ruthenium catalysts. *J. Catal.* **42**, 197–204 (1976).

188. Hunter, S. M. *et al.* A study of $^{15}\text{N}/^{14}\text{N}$ isotopic exchange over cobalt molybdenum nitrides. *ACS Catal.* **3**, 1719–1725 (2013).

189. Shannon, S. L. & Goodwin, J. G. Characterization of Catalytic Surfaces by Isotopic-Transient Kinetics during Steady-State Reaction. *Chem. Rev.* **95**, 677–695 (1995).

190. Nwalor, J. Steady-state isotopic transient-kinetic analysis of iron-catalyzed ammonia synthesis. *J. Catal.* **117**, 121–134 (1989).

191. Nwalor, J. U. & Goodwin, J. G. Isotopic tracing study of K promotion of NH₃ synthesis on Ru. *Top. Catal.* **1**, 285–293 (1994).

192. McClaine, B. Isotopic Transient Kinetic Analysis of Cs-Promoted Ru/MgO during Ammonia Synthesis. *J. Catal.* **210**, 387–396 (2002).

193. McClaine, B. C. & Davis, R. J. Importance of Product Readsorption during Isotopic Transient Analysis of Ammonia Synthesis on Ba-Promoted Ru/BaX Catalyst. *J. Catal.* **211**, 379–386 (2002).

194. Siporin, S. Isotopic transient analysis of ammonia synthesis over Ru/MgO catalysts promoted by cesium, barium, or lanthanum. *J. Catal.* **222**, 315–322 (2004).

195. Schlesinger, W. & Hartley, A. A global budget for atmospheric NH₃. *Biogeochemistry* **15**, 191–211 (1992).

196. Vojvodic, A. *et al.* Exploring the limits: A low-pressure, low-temperature Haber-Bosch process. *Chem. Phys. Lett.* (2014) doi:10.1016/j.cplett.2014.03.003.

197. Spinelli, J. B., Kelley, L. P. & Haigis, M. C. An LC-MS Approach to Quantitative Measurement of Ammonia Isotopologues. *Sci. Rep.* **7**, 10304 (2017).

198. Liu, Y. *et al.* Facile All-Optical Method for In Situ Detection of Low Amounts of Ammonia. *iScience* **23**, 101757 (2020).

199. Mou, S., Wang, H. & Sun, Q. Simultaneous determination of the three main inorganic forms of nitrogen by ion chromatography. *J. Chromatogr. A* **640**, 161–165 (1993).

200. Timmer, B. H., van Delft, K. M., Otjes, R. P., Olthuis, W. & van den Berg, A. Miniaturized measurement system for ammonia in air. *Anal. Chim. Acta* **507**, 137–143 (2004).

201. Kim, K., Yoo, C.-Y., Kim, J.-N., Yoon, H. C. & Han, J.-I. Electrochemical Synthesis of Ammonia from Water and Nitrogen in Ethylenediamine under Ambient Temperature and Pressure. *J. Electrochem. Soc.* **163**, F1523–F1526 (2016).

202. Sato, K. *et al.* A low-crystalline ruthenium nano-layer supported on praseodymium oxide as an active catalyst for ammonia synthesis. *Chem. Sci.* **8**, 674–679 (2017).

203. Chang, F. *et al.* Alkali and Alkaline Earth Hydrides-Driven N₂ Activation and Transformation over Mn Nitride Catalyst. *J. Am. Chem. Soc.* **140**, 14799–14806 (2018).

204. Kitano, M. *et al.* Low-Temperature Synthesis of Perovskite Oxynitride-Hydrides as Ammonia

Synthesis Catalysts. *J. Am. Chem. Soc.* (2019) doi:10.1021/jacs.9b10726.

205. Kitano, M. *et al.* Self-organized Ruthenium-Barium Core-Shell Nanoparticles on a Mesoporous Calcium Amide Matrix for Efficient Low-Temperature Ammonia Synthesis. *Angew. Chemie Int. Ed.* **57**, 2648–2652 (2018).
206. Ogura, Y. *et al.* Efficient ammonia synthesis over a Ru/La 0.5 Ce 0.5 O 1.75 catalyst pre-reduced at high temperature. *Chem. Sci.* **9**, 2230–2237 (2018).
207. Singh, A. R. *et al.* Electrochemical Ammonia Synthesis—The Selectivity Challenge. *ACS Catal.* **7**, 706–709 (2017).
208. Hodgetts, R. Y. *et al.* Refining Universal Procedures for Ammonium Quantification via Rapid ^1H NMR Analysis for Dinitrogen Reduction Studies. *ACS Energy Lett.* **5**, 736–741 (2020).

Glossary Terms

Activation barriers: The minimal amount of energy required for reactants to undergo a chemical reaction.

Standard potential: The potential of a reversible electrode at standard state with ions at an effective 1 M concentration at the pressure of 1 atm.

Electrochemical half-cell reactions: Either an oxidation reaction on the anode electrode where an electron is lost or a reduction reaction on the cathode electrode where an electron is gained.

Electric arc-generated hot plasma: A discharge of electric current across a spatial gap, sustained by the presence of a thermally ionized plasma, which allows for the flow of said current.

Reaction orders: the power dependence of the rate on the concentration of each reactant, which is an experimentally determined parameter that can have fraction values.

Tafel analysis: is used to determine an electrochemical systems transfer coefficient via voltammograms, thereby providing information about the electrochemical mechanism and catalytic activity.

Ohmic correction: Accounting for the Ohmic resistance of the media to accurately determine the potential at the surface of the electrode.

Quantum yield: Determining the number of times a specific event occurs per absorbed photon by the system in question.

Density functional theory: a computational quantum mechanical modelling method used to investigate the electronic structure of many-body systems.

Zero point energy: The lowest possible energy that a quantum mechanical system contains, which includes fluctuations in the lowest energy state from the Heisenberg uncertainty principle.